Solid Earth, 15, 1203–1231, 2024
https://doi.org/10.5194/se-15-1203-2024

Solid Earth Open Access EGU

Geomorphic expressions of active rifting reflect the role of structural inheritance: a new model for the evolution of the Shanxi Rift, northern China

Malte Froemchen[1], Ken J. W. McCaffrey[1], Mark B. Allen[1], Jeroen van Hunen[1], Thomas B. Phillips[1], and Yueren Xu[2]

[1]Department of Earth Sciences, Durham University, Science Labs, Durham, DH1 3LE, UK
[2]Key Laboratory of Earthquake Prediction, Institute of Earthquake Forecasting, China Earthquake Administration, Beijing, China

Correspondence: Malte Froemchen (malte.froemchen@durham.ac.uk)

Received: 31 October 2023 – Discussion started: 28 November 2023
Revised: 24 June 2024 – Accepted: 10 July 2024 – Published: 30 September 2024

Abstract. Many rifts are influenced by pre-existing structures and heterogeneities during their evolution, a process known as structural inheritance. During rift evolution, these heterogeneities may aid rift nucleation, rift growth, and the segmentation of faults; encourage the linkage of various segments; or even inhibit the formation of faults. Understanding how structural inheritance influences early rift evolution could be vital for evaluating seismic risk in tectonically active areas. The Shanxi Rift in the north of China is an active rift system believed to have formed along the trend of the Proterozoic Trans-North China Orogen; however, the influence of these pre-existing structures on the present-day rift architecture is poorly understood. Here, we use tectonic geomorphological techniques, e.g. the hypsometric integral (HI), channel steepness (k_{sn}), and local relief, to study the evolution of the Shanxi Rift and identify areas of higher tectonic activity. We found that the HI was less sensitive to lithology and more valuable in evaluating the tectonic signal and that activity is concentrated in two rift interaction zones (RIZs) formed between the Xinding, Taiyuan, and Linfen basins. We then evaluated the relationship between the active faults and mapped pre-existing structures, finding that many faults formed parallel to inherited structures, while faults in the RIZs often cross-cut these structures. Based on these observations, we propose a new model for the evolution of the Shanxi Rift, where inherited structures play an important role in the initial segmentation of the rift, which, in turn, controls the development of the RIZ structures.

1 Introduction

Many continental rifts exploit ancient orogenic belts to accommodate extensional strain. Examples include the East African Rift (Rosendahl, 1987; Morley, 1988; Ring, 1994), the Baikal Rift (Petit et al., 1996), and the Upper Rhine Graben (Schumacher, 2002). Research has focused on understanding the relationship between old northern pre-rift structures and how these old structures control the development of younger structures. Pre-existing orogenic belts influence the accommodation of subsequent episodes of extensional strain due to the presence of discrete and mechanically weak structures, such as shear zones and associated metamorphic fabrics (McCaffrey, 1997; Phillips et al., 2016; Fazlikhani et al., 2017; Kolawole et al., 2018; Peace et al., 2018; Heilman et al., 2019), pre-existing fault networks (Holdsworth et al., 2001), and lithological contacts (Wedmore et al., 2020; Phillips and McCaffrey, 2019). These mechanical-strength contrasts are particularly significant where orogenic belts are adjacent to cratons (Dunbar and Sawyer, 1988; Ziegler and Cloetingh, 2004; Corti et al., 2013), as is the case for the Baikal Rift (Petit et al., 1996), the East African Rift (Versfelt and Rosendahl, 1989), and the circum-Ordos rifts in China (Xu and Ma, 1992; Su et al., 2021), because the cratonic lithosphere is more resistant to deformation than younger orogenic belts.

Studies of the interaction between rift-related normal faults and inherited structures in offshore basins and margins use high-resolution 2D and 3D seismic-reflection data to analyse the influence of inheritance on the spatio-temporal

patterns of rift evolution (Morley et al., 2004; Phillips et al., 2016; Peace et al., 2018; Mulaya et al., 2022). Detailed field studies, on the other hand, can resolve the kinematic response of faults and infer strain field directions and interactions (e.g. East Africa; Hodge et al., 2018b; Wedmore et al., 2020; Heilman et al., 2019; Kolawole et al., 2018). Inherited structures and heterogeneities can influence the location, morphology, segmentation, and orientation of an entire rift zone (Wilson, 1966; Tommasi and Vauchez, 2001; Şengör et al., 2019; Heron et al., 2019; Schiffer et al., 2020; Kolawole et al., 2022). They can also influence the geometry and kinematics of individual faults (Wedmore et al., 2020; Samsu et al., 2020; Wilson et al., 2010). Inherited structures can influence the development of rifts and their associated basins by controlling the linkage of fault segments (Brune et al., 2017; Heilman et al., 2019). Pre-existing structures have also been shown to act as barriers to rift faults if they form structures or regions of strengthened crust that are harder to deform than surrounding areas (Krabbendam and Barr, 2000; Phillips and McCaffrey, 2019).

Many rifts that show a strong influence of inheritance are very segmented and exhibit numerous faults and basins that vary in terms of orientation and morphology (Morley et al., 2004; Reeve et al., 2015; Heron et al., 2019; Osagiede et al., 2020). Between individual basins of a rift zone, a complex deformation zone, known as a rift interaction zone (RIZ), may develop (Nelson et al., 1992; Koehn et al., 2008; Aanyu and Koehn, 2011; Sachau et al., 2016; Kolawole et al., 2021a). The morphology of this type of zone is principally controlled by the separation distance between fault segments, the polarity of the respective faults, and the amount of overlap between them (Morley et al., 1990; Faulds and Varga, 1998; Zwaan and Schreurs, 2017; Zwaan et al., 2016). RIZs are classified based on their geometrical organisation – i.e. whether rift segment faults "underlap" or overlap, or whether they are parallel, oblique, or orthogonal. Commonly, these zones are topographically distinct from the rest of the rift. RIZs may form topographic highs in their early evolution, functioning as a drainage divide between depocentres (Ebinger et al., 1987; Lambiase and Bosworth, 1995; Gawthorpe and Hurst, 1993) and therefore acting as a source of sediment (Gawthorpe and Hurst, 1993; Scholz, 1995). As RIZs evolve, they can become breached and eventually link up the rift basins (Kolawole et al., 2021a). RIZs can also be classified based on their evolution stage (Kolawole et al., 2021a), i.e. whether the RIZ is unbreached, partially breached, recently breached, or breached. This is assessed based on two observations: (1) the presence of a breaching fault that extends from one rift segment to the other segment and (2) the presence of an established physical linkage between depositional environments of both rift segments (i.e. a drainage connection between both segments). Recently breached and breached RIZs have an established breaching fault and connect the drainage of two different rift segments, but breached RIZs show less topography due to increased subsidence over the longer time period since the RIZ was breached. Unbreached RIZs show no apparent structural connection and no drainage connection, while partially breached RIZs may have a breaching fault that partially connects the rift basins, although drainage integration has not occurred yet. RIZs may also show a perturbed local strain field due to the influence of the adjacent, bounding rift faults (Crider and Pollard, 1998; Kattenhorn et al., 2000; Maerten, 2000; Kolawole et al., 2024). The development of these zones may be aided by basement fabrics that strike obliquely relative to the main extension direction (Fossen and Rotevatn, 2016); however, basement fabrics may also influence linkage across these zones (Morley et al., 2004; Heilman et al., 2019; Kolawole et al., 2021a). RIZs are important structural domains along rift systems, and inheritance may be key to understanding their geometry and evolution.

The Shanxi Rift is part of a Cenozoic rift system known as the circum-Ordos rifts; this system surrounds the Western Block of the North China Craton (NCC) (Fig. 1). Due to the strong lithosphere of the cratonic Western Block of the NCC, deformation was localised in two rift systems along it: the Weihe–Shanxi rift system in the southeast and the Yinchuan–Hetao rift system in the northwest (Zhang et al., 2003). The timing of the initiation of these rifts is debated as some authors argue for an Eocene–Oligocene initiation of the Weihe, Hetao, and Yinchuan rifts, with the Shanxi Rift being younger (Zhang et al., 2003; Shi et al., 2020), while other authors argue for a Late Miocene initiation for all rifts (Yin, 2010). The Shanxi Rift in northern China contains faults with a variety of trends that formed from the Late Miocene to the present day (Su et al., 2023) (Fig. 1). The origin of these trends is unclear, but the currently accepted model postulates that there have been multiple changes in stress axis orientation during the transtensional evolution of the Shanxi Rift since the Late Miocene, with strain being partitioned into dip-slip and strike-slip fault systems during transtension (Shi et al., 2015b). There has been little focus on the influence of structural inheritance on the wider evolution of northern China, with a few exceptions showing that active normal faults often follow the trends of inherited structures (Su et al., 2021) and possibly detach into low-angle shear zones at depth (Pavlides et al., 1999). Major faults in the Shanxi Rift commonly expose basement massifs of the Trans-North China Orogen (TNCO) in their footwalls. The TNCO formed during the collision of the Eastern and Western Blocks of the NCC in the Paleoproterozoic. While these basement massifs have been intensively studied to unravel the exact timing and kinematics of the Proterozoic collision (Kusky and Li, 2003; Zhao et al., 2005; Trap et al., 2007, 2008, 2009a, b; Faure et al., 2007; Zhai et al., 2010; Zhai and Santosh, 2011), their impact on late Cenozoic rifting in the Shanxi Rift has not been considered in detail.

There are limited seismic-reflection data available for the Shanxi Rift (Xu et al., 1993; Ai et al., 2019). However, the degree of tectonic activity and sub-aerial exposure makes it

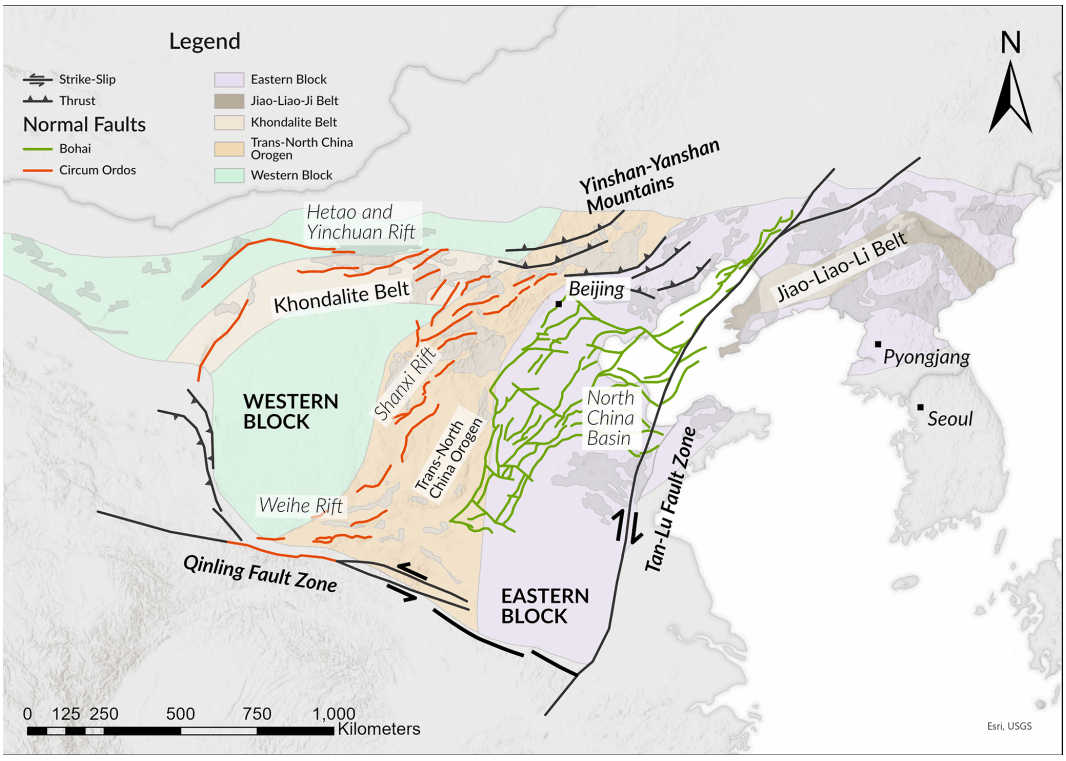

Figure 1. Overview map of the North China Craton (NCC), with the boundaries of the different blocks and orogenic belts that make up the NCC shaded in various colours. Boundaries are based on Zhao et al. (2005). Also indicated are the two major rift systems that formed, which are superimposed on the NCC: the Paleogene North China Basin (green; modified from Qi and Yang, 2010) and the Neogene circum-Ordos rifts (red; modified from Zhang et al., 2003; Deng et al., 2007). Bold black lines indicate the major strike-slip fault zones that influence present-day deformation.

possible to use geomorphology to study the structural evolution. In active rifts, geomorphology and surface expression of faults have been commonly used to study the tectonic evolution of a rift and have been successfully employed in regions such as the Basin and Range Province (Jackson and Leeder, 1994; Densmore et al., 2003, 2004), the Apennines (Whittaker et al., 2008; Geurts et al., 2020; Fisher et al., 2022), the Gulf of Corinth (Leeder and Jackson, 1993; Goldsworthy and Jackson, 2000; Fernández-Blanco et al., 2020; Gallen and Fernández-Blanco, 2021), and the East African Rift (Erbello et al., 2022; Dulanya et al., 2022). These geomorphic approaches vary and include studying drainage evolution and topographic responses to faulting and using rivers to track the transient uplift rate. Landscapes are primarily formed by two competing forces: tectonics and erosion (Whittaker, 2012). Geomorphic indices have been used to quantify landscape responses to tectonics (Bull and McFadden, 1980; Cox, 1994; Hamdouni et al., 2008; Gao et al., 2016; Makrari et al., 2022). This study uses three indices – the hypsometric integral, channel steepness, and local relief – to evaluate the landscape response to faulting in the Shanxi Rift.

Using geomorphic analysis to evaluate the tectonic evolution of the Shanxi Rift, highlight areas of increased tectonic activity, and compare these with the distribution of inherited structures, we provide new insights into the influence of inheritance on the evolution of the Shanxi Rift. Specifically, our results question the need for rapid changes in the Neogene strain field orientation to explain the varying fault orientations and fault evolution in the Shanxi Rift. Instead, we show a novel, simpler model in which inheritance under a constant strain field creates a segmented rift system and creates RIZs where strain and earthquake activity are focused. More generally, our work shows how geomorphic indicators can be used to identify the most active (and potentially hazardous) faults in an active extensional system.

2 Geological setting

The Shanxi Rift System in northern China is an active continental rift system superimposed on the 1.8 Ga TNCO (Fig. 1), which formed when the Eastern and Western Blocks collided to form the NCC. The exact timing and kinematics of this collision remain uncertain (Zhao et al., 2005; Kusky et al., 2007; Zhai and Santosh, 2011). Since the Proterozoic, the NCC has been a stable cratonic block with a lithospheric thickness of 200 km, as evidenced by Paleozoic kimberlites (Menzies et al., 1993; Griffin et al., 1998;

Menzies et al., 2007). Paleoproterozoic and Archean basement rocks are unconformably overlain by metasedimentary rocks (greenschist facies; Faure et al., 2007) of the Paleoproterozoic Hutuo Group, which were deposited in a foreland basin during the TNCO (Li et al., 2010). The lower Paleozoic cover consists of Cambrian continental siliclastic successions, followed by shallow marine carbonates and Ordovician platform carbonates. Carboniferous and Permian rocks were deposited under conditions varying from shallow marine to fluvio-deltaic and contain coal measures. These are topped by Mesozoic continental clastics, grading into cross-bedded aeolian sequences in the Jurassic (SBGMR, 1989). This evolution has led to a clear division of lithologies in the Shanxi Rift. The first group comprises Paleoproterozoic rocks, which include all the rocks that made up the TNCO, including Archean tonalite–trondhjemite–granodiorite complexes, high-grade metamorphic rocks (e.g. greenstone belts and orthogneisses), and post-orogenic granites. These rocks are referred to as Paleoproterozoic crystalline rocks in this study (dark-brown areas in Fig. 3) and are very resistant to erosion. The second group comprises the cover sequence of these rocks and is principally composed of low-grade metamorphic rocks, such as clastic metasediments and carbonates from the Mesozoic and Paleozoic eras, which are referred to as low-grade metasediments in this study (blue and green areas in Fig. 3).

Since the Mesozoic, parts of the NCC have been removed by thermal erosion (Griffin et al., 1998; Menzies and Xu, 1998) and/or partial delamination (Gao et al., 2002, 2004), which is likely related to the subduction of the Paleo-Pacific underneath East Asia (Menzies et al., 2007; Zhu et al., 2012). The eastern and western parts of the NCC underwent different evolutions during the Mesozoic. The eastern part experienced compressive deformation from the Jurassic to the Early Cretaceous (Davis et al., 2001), regionally known as the Yanshanian movement (Wong, 1927; Dong et al., 2015), which was less pronounced within the Western Block of the NCC. However, Paleoproterozoic orogenic belts, such as the TNCO, also recorded this widespread compressional event (Zhang et al., 2008, 2011; Clinkscales and Kapp, 2019). Since the Early Cretaceous, the eastern part of the NCC has experienced extension, resulting in structures such as pull-apart basins, core complexes, and associated voluminous magmatism (Zhu et al., 2012). Destruction of the cratonic lithosphere was limited to the eastern NCC, resulting in Mesozoic magmatism almost exclusively affecting the eastern NCC (Zhu et al., 2012). Here, the North China Basin formed in the Eocene–Oligocene (Allen et al., 1997). This basin exhibits transtensional kinematics, which means it resembles a giant pull-apart basin (Chen and Nabelek, 1988; Farangitakis et al., 2020). During the Paleogene, the western part of the NCC experienced limited extension. The Shanxi Rift is one of a series of narrow Neogene rifts which follow the trend of Precambrian orogenic belts within the NCC, developing around the Ordos Block (Shi et al., 2020).

The Shanxi Rift is an NE–SW-trending rift system that consists of a series of left-stepping en echelon basins (Zhang et al., 2003) (Fig. 2). The system is ~ 1000 km long and ~ 300 km wide and is bounded to the north by the Yinshan–Yanshan range and to the south by the Qin Mountains ("Qinling Fault Zone" in Fig. 1). It is commonly believed to have been initiated in the Late Miocene, based on the oldest sediments found in the rift grabens – the Kouzhai formation (Xu et al., 1993). The crust beneath the Shanxi Rift is ~ 32–39 km thick and is thinner in the basinal regions compared to the areas adjacent to the highlands of the Lüliang and Taihang mountains, which flank the rift to the west and east (Chen, 1987; Tang et al., 2010). The Shanxi Rift is characterised by a series of distinct rift basins with either half-graben or graben geometries, separated by two higher, topographically elevated areas, which have previously been called push-up swells but are referred to here as RIZs (Fig. 2) (Xu and Ma, 1992; Xu et al., 1993). The Linfen Basin, located to the south, is separated from the Taiyuan Basin by the Lingshi RIZ; in turn, the Taiyuan Basin is separated from the Xinding Basin, located in the north, by the Shilingguan RIZ. There are two main rivers that drain the Linfen–Taiyuan–Xinding basin system of the Shanxi Rift: the Hutuo River, which flows east across the Xizhoushan fault into the North China Plain, and the Fen River, which is diverted to the south, where it drains into the Yellow River (Fig. 2). The main drainage divide between the Fen and Hutuo rivers is represented by the Shilingguan RIZ. The syn-rift thickness across the Shanxi Rift varies: while the Taiyuan Basin has the greatest syn-rift sediment thickness, up to 3800 m (Xu et al., 1993), the Xinding Basin only has a thickness up to 1800 m (Xu et al., 1993), and the Linfen Basin contains up to 2200 m of syn-rift fill (Su et al., 2023). The Shanxi Rift shows widespread seismicity for M_{w} 3–5 events on USGS and International Seismological Centre (ISC) records (Fig. 2), but the rift has produced infrequent yet devastating earthquakes in historical times. The 1303 Hongdong earthquake is believed to have been an $M_{\mathrm{W}} \sim 7.5$ event (Xu et al., 2018) and is well documented in Chinese historical writings. The province of Shanxi is densely populated, with 36.5 million inhabitants. Large cities like Taiyuan (5 million inhabitants), Linfen (4 million inhabitants), and Datong (3 million inhabitants) are close to active faults (Fig. 2)

Constraining the exact extension direction and rate along extensional faults is difficult due to the Shanxi Rift's low extensional-strain rate. Research has been conducted based on field-based fault slip measurements, GPS-derived velocities, and/or earthquake focal mechanisms to constrain the extension direction. Studies by Shen et al. (2000), He et al. (2003), and Middleton et al. (2017) constrain the extension direction in the Shanxi Rift to ~ 105–$165°$ and the extension rate to ~ 0–$6\,\mathrm{mm\,yr^{-1}}$ (Fig. 2). Other studies using field-based measurements (Shi et al., 2015b; Assie et al., 2022) propose a complex, evolving strain field that has changed throughout the Cenozoic. According to these stud-

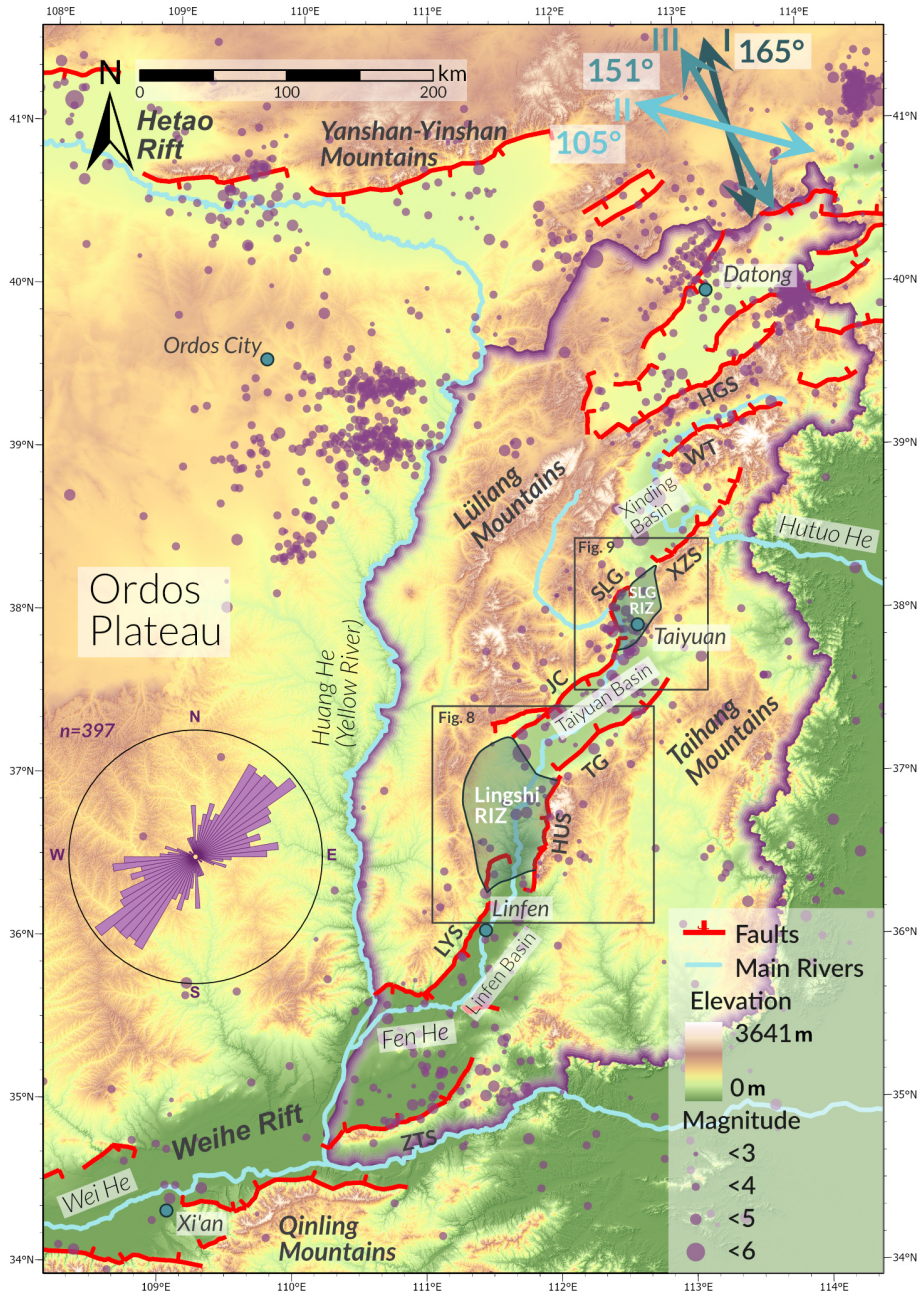

Figure 2. Detailed map of the circum-Ordos rifts and the main rivers. Extension directions are from (I) Zhang et al. (1998), (II) Shen et al. (2000), and (III) Middleton et al. (2017). The rose plot shows the mean orientation of major rift faults in the Shanxi Rift (defined here as the region that lies within the purple boundary line). Faults were split into individual segments according to their orientation. Purple dots represent earthquakes from the ISC catalogue (Storchak et al., 2013, 2015; Di Giacomo et al., 2018) and are weighted by magnitude. HGS: Hengshan. WT: Wutai. XZS: Xizhoushan. SLG: Shilingguan. JC: Jiaocheng. TG: Taigu. HUS: Huoshan. LYS: Luoyunshan. ZTS: Zhongtiaoshan.

ies, NW–SE extension in the Mio-Pliocene initiated rifting in Shanxi and was followed by NE–SW extension in the early Quaternary, leading to further subsidence. Theses authors suggest that the onset of the current NNW–SSE extension strain field started at 0.11 Ma and marked a shift from NW–SE extension to right-lateral deformation in the Shanxi Rift, as dated using faulted basalts in the Datong Basin (Shi et al., 2015b). Shi et al. (2015a, b) relate these changes in the strain field to the growth of the Tibetan Plateau.

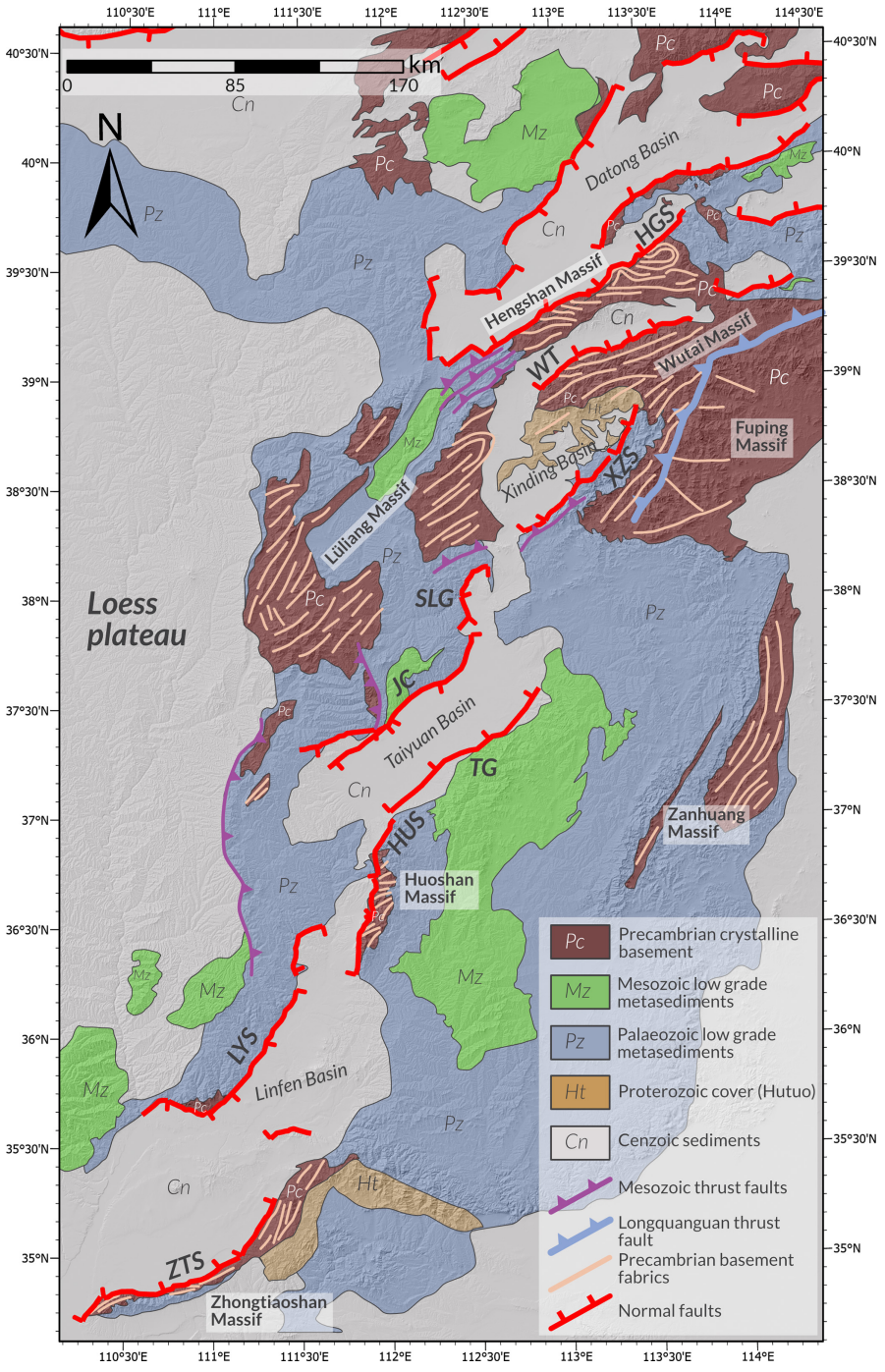

Figure 3. Simplified geological map of the Shanxi Rift (modified from SBGMR, 1989, and Clinkscales et al., 2021) showing the main structures (Faure et al., 2007; Trap et al., 2007, 2009a, b; Zhang et al., 2011; Clinkscales and Kapp, 2019). The main metamorphic fabrics are indicated by grey lines, which are predominantly oriented NE–SW.

3 Methods

3.1 Pre-rift architecture and structural mapping

We compiled a map of the structures in the Shanxi Rift (Fig. 3) by digitising Precambrian basement fabrics, Mesozoic and Precambrian thrust faults, and Cenozoic active faults from published maps in ArcGIS Pro™. Additionally, we compiled published structural data from the Paleoproterozoic basement complexes for plotting on stereonets (Fig. 4). In this study, we primarily focus on the influence of inherited structures in the Paleoproterozoic basement on

the evolution of the Shanxi Rift; therefore, unless specified otherwise, we refer to Paleoproterozoic structures when discussing basement or inherited fabrics. To map the active fault structures, we identified linear breaks in the landscape using Shuttle Radar Topography Mission (SRTM) topographic data with a 90 m resolution (https://lpdaac.usgs.gov/products/srtmgl3v003/, last access: 14 September 2024), aided by slope and curvature attributes. This resolution is appropriate for the larger regional scale of this study and helped keep computing-power demands manageable. We define active faults as steep, linear scarps (> 20–30°) that offset Quaternary sediments, similar to the approach used by Wedmore et al. (2022). Furthermore, we used topographic profiles across faults and geomorphological features, such as steepened river channels and triangular facets along the fault scarp, to guide our identification of active normal faults.

3.2 Geomorphic indices

We used geomorphic indices to quantify the landscape response of the Shanxi Rift to tectonic drivers. We analysed the morphometric indices from 10 873 first-order drainage basins located in the Shanxi Rift, extracted from the SRTM dataset using MATLAB scripts from TopoToolbox v2 (Schwanghart and Scherler, 2014). In this study, we focused on three geomorphic indices – (1) local relief (R_l) (Fig. 5a), (2) normalised channel steepness (k_{sn}) (Fig. 5b), and (3) the hypsometric integral (HI) (Figs. 5c and 6) – as these indices proved to be the most helpful and discerning when evaluating tectonic signals (Pérez-Peña et al., 2009; Gao et al., 2016; Obaid and Allen, 2019; Groves et al., 2020; Erbello et al., 2022). Using R, we also generated violin plots to visualise the distribution of values for each geomorphic index (Fig. 7). The shape of the "violins" represents the distribution of values as the violin is thicker in the ranges where more data points cluster. Using these violin plots, we can also assess the impact of lithology on the geomorphic indices, enabling us to compare the distribution of values per fault with the dominant footwall geology of the fault, and assess whether lithology is the principal factor determining the distribution.

3.2.1 Local relief (R_l)

Local relief is commonly used for measuring variation in topography over an area and is used to analyse spatio-temporal tectonic trends (Ahnert, 1970; Schmidt and Montgomery, 1995; DiBiase et al., 2010). The relief (R_l) was calculated as the maximum difference in elevation (E) over a delineated drainage basin (Fig. S1 in the Supplement) or within a circular moving window with a 1 km radius and is given as follows:

$$R_l = E_{max} - E_{min}, \quad (1)$$

where R_l is the local relief and E refers to elevation. High-relief landscapes therefore show higher variation in elevation over an area, which may indicate faster uplift rates. However, although local relief is influenced by lithology, high-relief landscapes can also be the result of resistant lithologies with low erodibility.

3.2.2 Normalised channel steepness (k_{sn})

Normalised channel steepness (k_{sn}) is a frequently used topographic metric in tectonic geomorphology (DiBiase et al., 2010; Whittaker and Walker, 2015). For steady-state landscapes, where rock uplift rates and river incision rates are in equilibrium, the channel slope (S) is defined as a power-law function (Hack, 1957; Flint, 1974), expressed as

$$S = k_s A^{-\theta}, \quad (2)$$

where A is the drainage area. The parameter k_s is the channel steepness index, and θ denotes the channel concavity index (Snyder et al., 2000). In natural landscapes, its well known that variations in the best-fit concavity index (θ) have a significant impact on estimates of k_s. To circumnavigate this problem, we used a reference concavity index of 0.45 (Wobus et al., 2006). This reference concavity index results in a dimensionless normalised channel steepness (k_{sn}). Variations in k_{sn} along channel segments may be related to changes in the uplift rate for that region (Snyder et al., 2000; Whipple, 2004), with higher k_{sn} values often indicating higher uplift rates.

We used the MATLAB scripts from TopoToolbox v2 (Schwanghart and Scherler, 2014) to extract the river profiles and calculate the normalised channel steepness from smoothed river profiles. This approach builds upon the method developed by Perron and Royden (2013) for analysing river profiles. We extracted streams with a drainage area of more than 1 km^2 to avoid hillslope areas. Normalised channel steepness (k_{sn}) is commonly applied to stream networks to visualise knickpoints (variations in the slope of river channels) in rivers. In this study, we used TopoToolbox v2 to calculate the basin-averaged k_{sn} values. This was achieved by calculating the mean of all k_{sn} values for each drainage basin, making it easier to compare k_{sn} values with local-relief and HI values. The k_{sn} stream network map is available in the Supplement (Fig. S2).

3.2.3 Hypsometric integral (HI)

The hypsometric integral (HI) was first used as a geomorphic index by Strahler (1952, 1957). It measures the distribution of elevation within an area. The HI is derived as the integral of the hypsometric curve, which plots normalised elevation against the normalised drainage area for each drainage basin. Figure 6 illustrates the theory behind the HI. The interpretation of the hypsometric curve assumes that topographically younger basins will exhibit a "convex-up" curve, while more mature ones will exhibit a more "concave-up" shape. If uplift exceeds erosion, there will be a greater range of eleva-

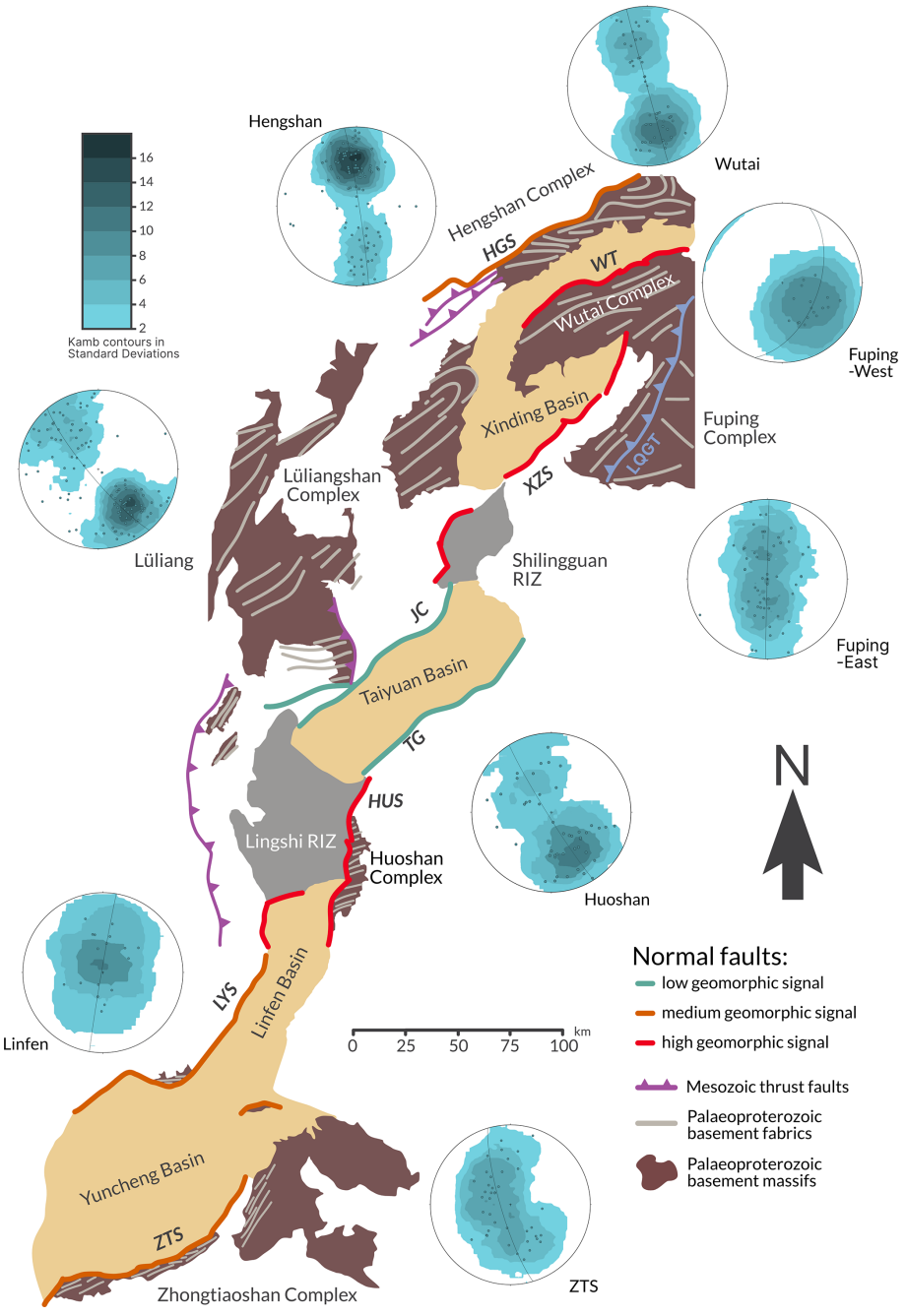

Figure 4. Schematic fault map of the Shanxi Rift, with faults colour-coded according to their geomorphic signal (compare with Table 1). The exposed basement of the TNCO is shown in brown, with the main structural trends highlighted in light grey. Stereonets illustrating poles to planes (data from Trap et al., 2007, 2009a) show the structural grain of the main basement complexes. Most basement complexes show an NE–SW-oriented grain, although this grain trends more E–W in the north.

tion over an area, which results in a convex-up curve and a high HI. Therefore, high HI values should correspond with rapidly uplifting areas (e.g. footwalls of active normal faults) (Hamdouni et al., 2008; Perez-Pena et al., 2009; Obaid and Allen, 2019; Groves et al., 2020; Erbello et al., 2022). The HI may be influenced by factors other than tectonic uplift, such as climate, lithology, basin shape, and basin area. Lifton and Chase (1992) propose that for analysis at larger scales (> 1000 km), tectonics will have a larger effect than lithology, while at smaller scales, lithology can have a considerable impact. Masek et al. (1994) suggest that climate can influence the hypsometry of an area. Several studies pro-

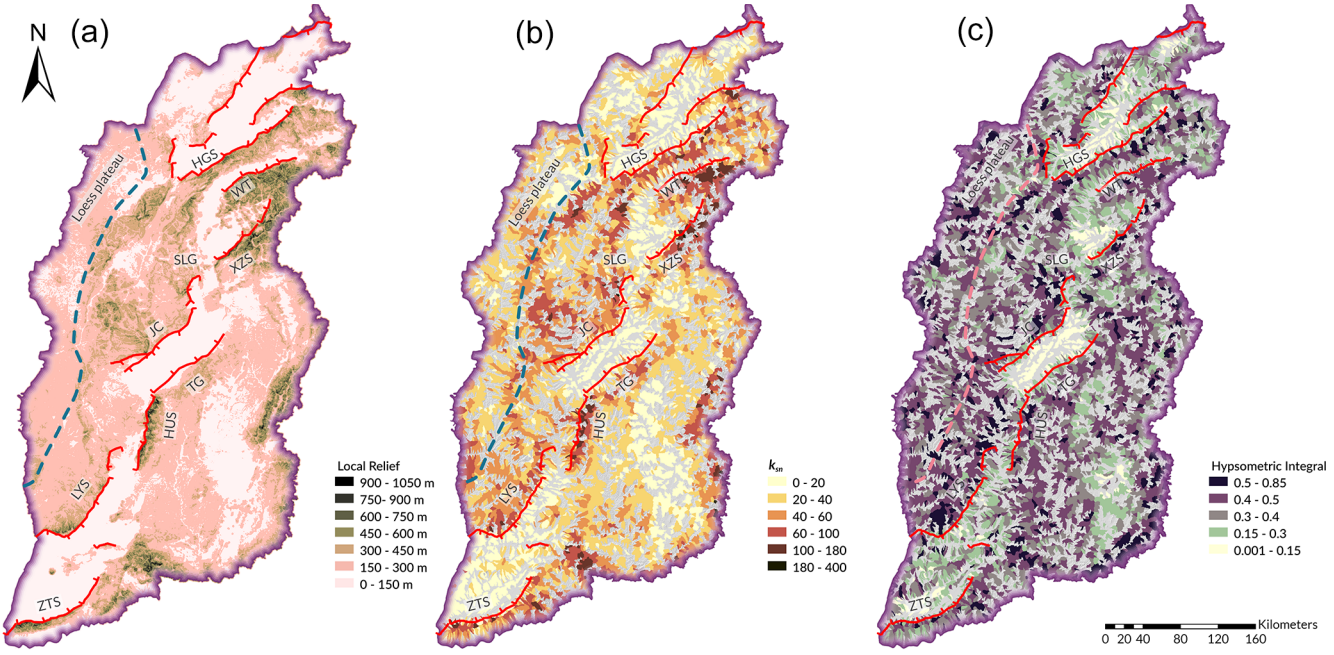

Figure 5. Geomorphic-index map of the Shanxi Rift. Major extensional faults are shown in red, and the boundary of the Loess Plateau is indicated by a dashed line. Panel **(a)** shows a local-relief map. Darker colours indicate higher-relief regions. Local relief was calculated within a 1 km circular radius. High relief is found particularly in the northern Shanxi Rift (in the footwalls of the Wutai and Xizhoushan faults and further south along the Huoshan and Zhongtiaoshan faults). Noticeably lower local-relief values are found along the central Jiaocheng and Taigu faults. Panel **(b)** shows mean normalised channel steepness (k_{sn}) calculated for first-order Strahler basins. High values are commonly observed in the footwalls of active faults, especially the Wutai, Xizhoushan, and Huoshan faults. Low values are observed in the lower-lying basin regions. Central faults (i.e. the Taigu and Jiaocheng faults) show noticeably fewer basins with high k_{sn} values than other faults. Panel **(c)** shows the hypsometric integral (HI) calculated for first-order Strahler basins. High values are commonly observed in the footwalls of active faults, especially the Wutai, Linfen, Shilingguan, and Huoshan faults. Low values are observed in the lower-lying basin regions. HGS: Hengshan. WT: Wutai. XZS: Xizhoushan. SLG: Shilingguan. JC: Jiaocheng. TG: Taigu. HUS: Huoshan. LYS: Luoyunshan. ZTS: Zhongtiaoshan.

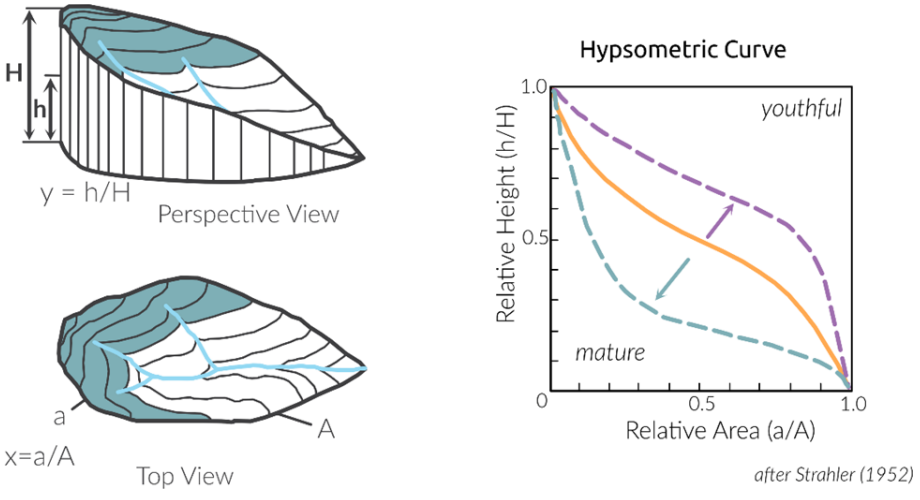

Figure 6. Schematic diagram explaining the concept of the hypsometric integral, based on Strahler (1952). Each drainage basin is divided into elevation bands to determine the ratio of relative height to relative area. Concave curves indicate more youthful topography, while convex ones indicate more mature topography.

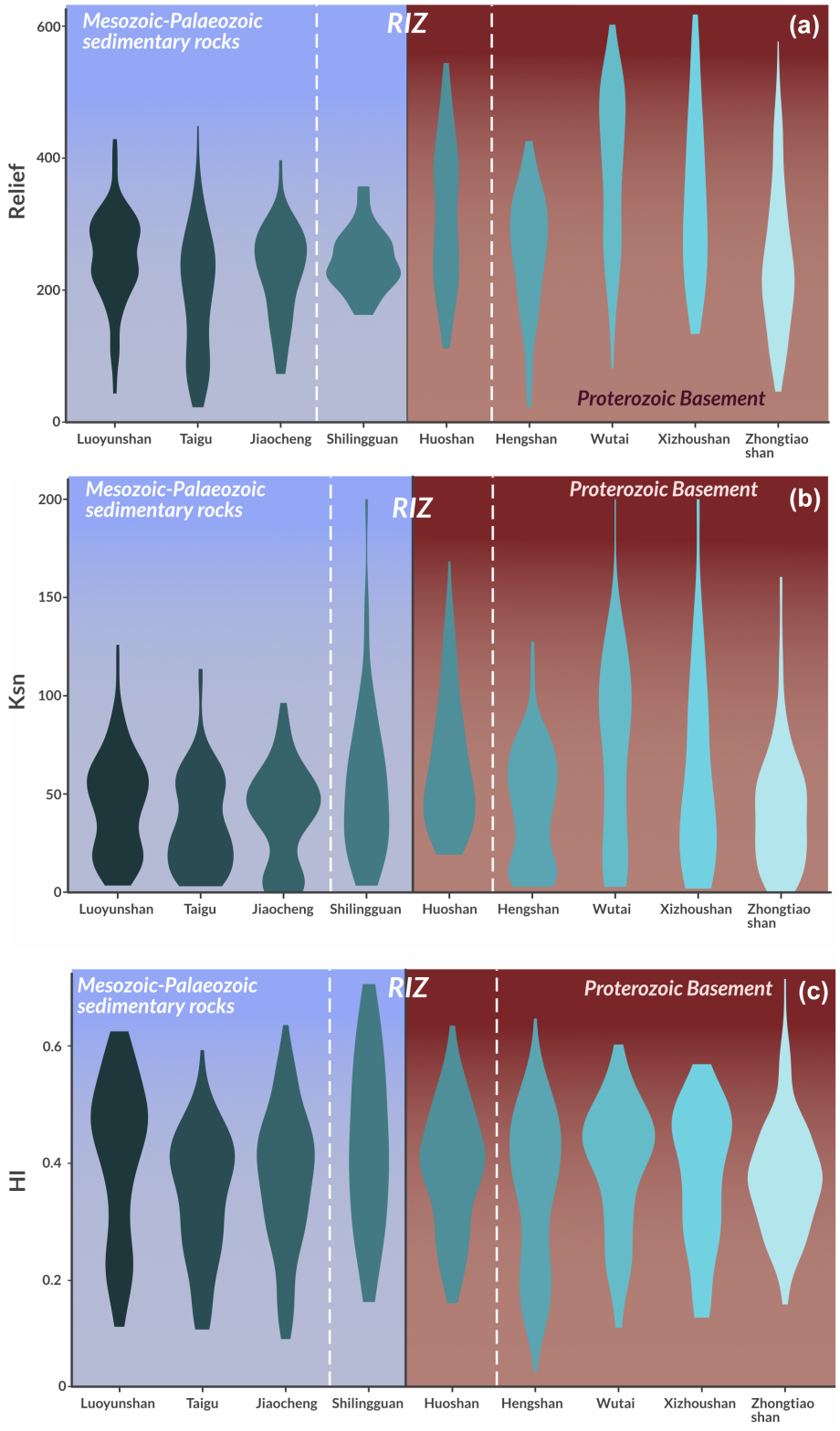

Figure 7. Violin plots showing the distribution of geomorphic values for each fault. The background shows the dominant footwall composition of the faults, with RIZ faults plotted in the middle. Panel **(a)** illustrates local relief. There is a clear separation, with faults exhibiting high values all having footwalls dominated by Proterozoic basement. Panel **(b)** displays k_{sn} values that show a similar separation to the mean relief. Panel **(c)** shows HI values that are more distributed. RIZ faults tend to have high geomorphic values (see the main text for more discussion on this).

pose that basin shape and area influence the HI of a basin (Lifton and Chase, 1992; Masek et al., 1994; Hurtrez et al., 1999; Chen et al., 2003). However, Walcott and Summerfield (2008) analysed the basins of southern Africa and found that the basin scale had no impact on the HI. High-HI regions are often indicative of fast uplift rates but can also be related to other factors. Therefore, when analysing the tectonic implications of the HI, it is important to be aware of these limitations. To mitigate the effect of lithology on our tectonic analysis, we also compare the HI distribution for each fault with the predominant lithology of the fault's footwall using violin plots generated with R (Fig. 7c).

In this study, we calculated the HI for each drainage basin (Obaid and Allen, 2019; Groves et al., 2020). The shape and size of drainage basins are controlled by tectonic and geological features. Therefore, drainage basins provide more natural boundaries for comparing areas of variable uplift and erosion rates than calculating the HI with an arbitrary moving window. We calculated the hypsometric curves using QGIS 3.16 and derived the integral for each curve through an R script (Froemchen et al., 2024).

4 Results

4.1 Pre-rift structural architecture

The northern part of the Shanxi Rift is dominated by uplifted Paleoproterozoic basement massifs. The Hengshan, Lüliang, Wutai, and Fuping massifs are exposed in the footwalls of major basin-bounding faults (Figs. 3 and 4). In the south, the footwalls are more commonly dominated by Mesozoic and Paleozoic sedimentary rocks, with notable exceptions being the Huoshan and Zhongtiaoshan faults, which also expose Paleoproterozoic metamorphic basement at the surface.

The general trend of most Paleoproterozoic structures is broadly NE–SW, which is sub-parallel to the active rift faults. In the northern basement massifs (i.e. the Hengshan and Wutai massifs), there is a subtle change to the WNW–ESE trends (Figs. 3 and 4). The dip of these structures is variable due to the folded nature of these rocks (Trap et al., 2007, 2009a; Clinkscales and Kapp, 2019). The dip of the fabrics varies along the strike, changing from dipping towards to dipping away from the faults, with a range from 25–85° (Trap et al., 2007, 2009a). The orientations also show plunging fold geometries in the basement massifs of Mount Heng and the Lüliang Mountains (stereonets of Hengshan and Lüliang in Fig. 4). The Fuping massif displays a considerable spread of basement fabric trends that can be split into two groups: fabrics trending NE–SW in the northwest and fabrics with an NNW–SSE trend in the southeast (stereonets of "Fuping-West" and "Fuping-East" in Fig. 4). These two regions are separated by the NE–SW-trending Longquanguan thrust fault (marked as a blue thrust fault in Figs. 3 and 4), which most likely originated as a shallow-dipping thrust fault in the Paleoproterozoic (Trap et al., 2008). The basement fabrics in the northwestern part and the Longguanquan thrust fault are parallel to the Xizhoushan fault ("Fuping-West" stereonet in Fig. 4). Further north, the Paleoproterozoic basement fabrics of the Wutai Complex are oriented ENE–WSW, which is mirrored by the active normal Wutai fault.

4.2 Relief

The local relief (Fig. 5a) closely follows the overall topography of the region but emphasises certain features to make them easier to identify. Two areas of high local relief can be identified in the north and south of the Shanxi Rift.

In the northern region around the Wutai and the Xizhoushan faults, the footwalls of the prominent bounding faults are highly elevated (2500–3000 m) and show local-relief values exceeding 1000 m. In the southern part of the Shanxi Rift, the Huoshan fault also shows high local-relief values ($>$ 1000 m) in its footwall, situated close to the bounding fault. These high-relief faults in Shanxi show consistently high local-relief values along their fault traces, whereas the Zhongtiaoshan fault exhibits high local-relief values ($>$ 1000 m) along the western end of the fault and lower values towards the east.

The Shilingguan RIZ is characterised by shorter fault segments, and this region shows an elevated local relief of around 500 m. In some examples, local relief exceeds 1000 m in footwalls close to the main fault. This is seen where a broadly N–S-trending fault intersects and links up with broadly NE–SW-trending fault. Further into the footwall of this fault, there are pockets of high ($>$ 1000 m) local relief, located along the sides of the narrow gorge of the Fen River. Compared to faults in the north and south of the Shanxi Rift, such as the Huoshan, Zhongtiaoshan, and Wutai faults, the elevation in this area is lower ($\sim$ 1500 m), but the local relief remains comparatively high (up to 1000 m). The two longest faults in the central region of the Shanxi Rift (i.e. the Taigu and Jiaocheng faults), which bound the Taiyuan Basin, show a lower local-relief response, rarely exceeding 450 m, with elevation lying between 1500 and 2000 m. There are regions of medium–high values of local relief (450–750 m) that are located away from active structures, e.g. in the Taihang Mountains or to the west of the Lingshi RIZ.

The distribution of relief values per fault (Fig. 7a) shows a clear divide between faults. The faults which have Proterozoic basement rocks in their footwalls (i.e. the Huoshan, Xizhoushan, Zhongtiaoshan, Hengshan, and Wutai faults) have a greater range of values, often exceeding 400 m. This is especially pronounced for the Wutai and Xizhoushan faults. The Hengshan fault is slightly different as its distribution of relief values is closer to that of the faults with Paleozoic–Mesozoic sedimentary rocks in their footwalls, with most values ranging from 200–300 m. The Zhongtiaoshan fault has a maximum value at around 200 m and, therefore, has lower relief compared to the other faults. However, it still has some val-

ues in the higher ranges, with a maximum value of 600 m. The faults with Paleozoic and Mesozoic sedimentary rocks in their footwalls (i.e. the Shilingguan, Taigu, Jiaocheng, and Linfen faults) have lower values overall and a smaller range of values. Most of their values lie between 200–300 m, but their minimum values are below 100 m. The Shilingguan fault, as the RIZ fault, shows a similar maximum at 200–300 m but lacks the low minimum values, resulting in a more compact distribution.

4.3 Normalised channel steepness (k_{sn})

Four regions show high basin-averaged k_{sn} values (Fig. 5b): the Huoshan fault, the Xizhoushan fault (especially its northeastern part), the Wutai fault, and the Zhongtiaoshan fault. These are the same regions that show high local relief (Fig. 5a; Sect. 4.2). Low values of < 50 are rarely associated with obvious faults with a surface trace. The Jiaocheng and Taigu faults' footwalls have drainage basins with k_{sn} values between 50–85, which reflects the local-relief response of these faults (Fig. 5a). The footwall of the fault bounding the Shilingguan RIZ shows elevated values. Notably, the area where the broadly N–S-striking and NE–SW-trending faults link up shows basins with $k_{sn} > 100$. The k_{sn} value distribution (Fig. 7b) of the different faults shows a similar trend to the local relief as there is a separation between faults with different basement lithologies. The faults with Proterozoic basement show much higher values, reaching values up to 200, while the faults with Paleozoic–Mesozoic basement show narrower distributions, rarely > 100 and with most values < 50. Notable outliers are found along the Hengshan fault, whose distribution, again, is more similar to that of the Paleozoic–Mesozoic basement faults. Here, the Shilingguan RIZ records higher values (> 100) than the other faults with Paleozoic–Mesozoic basement footwalls and has a distribution more similar to that of the faults with Proterozoic basement footwalls, such as the Wutai or Xizhoushan faults.

4.4 HI

While the local relief and channel steepness show broadly similar distributions, the HI differs slightly, resulting in a more distributed pattern of basins with a high HI (> 0.5; Fig. 5c). The footwall blocks of the Wutai, Xizhoushan, and Zhongtiaoshan faults show elevated responses, but, in contrast to the previously described geomorphic parameters, they do not show the highest values. In the footwalls of these faults, HI values mostly range between 0.3–0.5, and only isolated regions show values > 0.5. The bounding fault of the Shilingguan RIZ has some of the highest HI responses, with values often exceeding 0.5 and rarely being below 0.4. The Lingshi RIZ, which is bounded by the Huoshan fault, also shows elevated values compared to the surrounding basins due to its overall higher elevation and dissected topography. These high HI values match spatially with the high local-relief and k_{sn} values. Therefore, the Shilingguan RIZ and Huoshan fault have consistently higher values compared to the Wutai, Zhongtiaoshan, and Xizhoushan footwalls. The Luoyunshan fault, adjacent to the Lingshi RIZ, also shows basins with an elevated HI (> 0.5), especially towards the southern end, where it exhibits a distinct fault bend; however, these high HI values do not match as well with local-relief and k_{sn} values (Sect. 4.2 and 4.3). The Taigu fault has lower HI values (< 0.4), matching the low values for channel steepness and local relief. The Jiaocheng fault not only has a greater spread with respect to low-value basins (0.2–0.4) but also has basins with higher HI values (0.5–0.85), especially towards the northeast of the fault, which is nearer the Shilingguan RIZ.

Basins with high HI values (> 0.5) are also found in regions more distant from the active normal faults that showed no recent tectonic activity. High values are observed to the west of the Shanxi Rift in the Loess Plateau, on the western edge of the HI map (Fig. 5c). Similar to the relief and channel steepness, high values are also observed in high-elevation regions further from mapped active faults. These commonly correspond to known thrust faults or other contractional structures (Fig. 3) (SBGMR, 1989), which were last active in the Mesozoic and created relict topography.

The distribution of HI values (Fig. 7c) significantly differs from that of the previous two geomorphic indices as a clear separation based on lithology and/or footwall age is not obvious anymore, and the patterns are more dispersed. The general trend still suggests that faults with Proterozoic basements have slightly higher values (~ 0.5); however, the Zhongtiaoshan fault, while reaching very high HI values, mostly has values around 0.4, which is lower than the values for the other faults with Proterozoic footwalls and closer to the values for faults with Paleozoic–Mesozoic sedimentary rocks in their footwalls. Among these faults, the Luoyunshan and Shilingguan faults show higher values than the Taigu and Jiaocheng faults. Overall, the Shilingguan and Huoshan faults, located within the RIZs, record the highest values, but they are not significantly elevated compared to, for example, the Wutai and Luoyunshan faults.

5 Discussion

The quantitative analysis of the geomorphic response of the main rift faults shows that the Wutai, Xizhoushan, Shilingguan, and Huoshan faults show the highest geomorphic response (Fig. 7; Table 1) and that they are classified by high HI values (mean HI > 0.35), k_{sn} values (mean $k_{sn} > 60$), and R_l values (mean $R_l > 250$). Of these, the Shilingguan and Huoshan faults are located within the RIZs and exhibit both N–S-trending and NE–SW-trending fault segments. The Taigu and Jiaocheng faults have the lowest geomorphic responses and show low values for all three geomorphic indices (mean HI < 0.3; mean $k_{sn} < 40$; mean $R_l < 200$). The Hengshan,

Zhongtiaoshan, and Luoyunshan faults fall in between these two groups and are described as faults with a medium geomorphic response in Table 1. In the following, we will discuss the significance of these results and the possible influence of the pre-existing structures described in Sect. 4.1.

5.1 Lithology dependence of geomorphic indices

The distribution of geomorphic indices for each fault shows significant differences (Fig. 7). Geomorphic response may be influenced by climate, lithology, and tectonics. The climate across Shanxi is continental and shows little variation in precipitation overall (Fig. S3; Fick and Hijmans, 2017) across the study region, which makes it unlikely that differences in geomorphology between faults are controlled by the climate. The lithology in Shanxi is more variable, as seen in Fig. 3. The various lithologies can be divided into two main groups that differ in terms of rock strength and erodibility. These are Precambrian crystalline rocks, which include Archean tonalite–trondhjemite–granodiorite complexes, high-grade metamorphic rocks, and post-orogenic granites (all part of the TNCO; Trap et al., 2012), and low-grade metasediment units, which include low-grade clastic metasediments and carbonates from the Paleozoic–Mesozoic (SBGMR, 1989). Here, we evaluate how these differences in lithology may have impacted the geomorphic response.

Local relief and k_{sn} (Fig. 5a and b) show the highest values at which crystalline-basement lithologies are exposed in the fault footwall. Faults with high mean local-relief values (> 300 m) have strong crystalline basement in their footwalls (e.g. the Huoshan, Wutai, and Zhongtiaoshan faults) or are directly adjacent to such faults (e.g. the Xizhoushan fault), while faults with Paleozoic–Mesozoic rocks in their footwalls (e.g. the Taigu and Jiaocheng faults) show low values ($\sim< 200$ m). The HI (Fig. 5c) does not show the same bimodal distribution between faults with different footwall lithologies. The highest HI values correspond to faults with both Proterozoic basement footwall rocks (e.g. the Huoshan, Wutai, and Xizhoushan faults) and Paleozoic–Mesozoic footwall rocks (e.g. the Shilingguan and Luoyunshan faults). Meanwhile, low HI values are also found for footwalls of both lithologies (e.g. in the Hengshan, Taigu, Jiaocheng, and Zhongtiaoshan faults). We can infer that the differences in HI values between these fault blocks are likely not due to their lithology but are rather due to their tectonic history. This suggests that the HI may be a more robust geomorphic index for analysing tectonic activity than relief or k_{sn} because it is less influenced by lithology. Our finding that the HI is not primarily influenced by lithology agrees with previous studies (Obaid and Allen, 2019; Groves et al., 2020). High HI values are often correlated with high uplift rates, especially in regions with variable uplift rates, and higher HI values are found in regions of higher uplift (Hurtrez et al., 1999). Therefore, the high HI values found in the footwalls of the Huoshan, Wutai, Xizhoushan, and Shilingguan faults indicate that these footwalls have been uplifted most rapidly.

Towards the western edge of the Shanxi Rift, there is a region of medium–high-HI basins that do not correlate with mapped active faults. This is likely due to the landscape typifying the Loess Plateau, located west of the Shanxi Rift. The Loess Plateau consists of unconsolidated windblown sediment that is prone to dramatic erosion, creating deep gullies and ridges, which can lead to high HI values. The Loess Plateau formed in the Pleistocene, and its linear ridges and gullies have been carved out by aeolian and fluvial forces (Kapp et al., 2015); therefore, the high HI response of the Loess Plateau is related to young landscapes sculpted by surface processes rather than tectonic forces. This does not detract from the main point that the HI is less influenced by lithology as the Loess Plateau represents an extreme case of unconsolidated sediment compared to the main groups of low-grade metasediments and Paleoproterozoic crystalline rocks. However, it does highlight that the HI response is sensitive to the presence of loess. When using the HI to evaluate the tectonic response of an area partially covered by loess, the fact that loess-covered areas may show anomalously high HI values must be considered.

The dependence of some geomorphic indices on lithology is observed in many other areas worldwide and highlights the importance of considering the local geology when interpreting the relevance of geomorphic indices (Wobus et al., 2006; Kirby and Whipple, 2012). However, by comparing different faults with similar basement geology, the lithological impact can be reduced as, theoretically, these faults should have similar rock strength and erodibility. This allows us to compare the landscape response of these footwall uplifts to tectonics. In the Shanxi Rift, the footwall of the Huoshan fault, on average, has higher values for geomorphic indices than other faults with Paleoproterozoic crystalline rocks in their footwalls (Fig. 7). Comparing the response of faults with footwall exposures of low-grade metasediment rocks, it becomes evident that the main bounding fault of the Shilingguan fault has a higher geomorphic response than the Jiaocheng, Luoyunshan, and Taigu faults. The difference in geomorphic response between the Shilingguan fault and the other faults with low-grade metasediments in their footwalls is even more pronounced than that between faults with Paleoproterozoic crystalline basement rocks. For example, the difference between the Huoshan and Hengshan faults is less stark than the difference between the Shilingguan fault and the Jiaocheng fault. It must also be noted that the Shilingguan fault shows higher HI and k_{sn} values than faults with "stronger" Paleoproterozoic crystalline rocks in their footwalls (i.e. the Hengshan and Zhongtiaoshan faults). By comparing faults with similar footwall lithologies, we can show that the difference in geomorphic response is not solely due to lithology and most likely has a tectonic origin.

Table 1. Summary of the faults and their geomorphological responses, as well as their lithology and the orientation of the inherited fabrics in the vicinity of the faults.

Shanxi Rift fault characteristics							
Fault	Trend (°)	Footwall lithology	Mean R_l	Mean HI	Mean k_{sn}	Geomorphic response	Orientation of inherited structures
Hengshan	57	Crystalline basement	234	0.33	68	Medium	E–W
Wutai	65	Crystalline basement	367	0.37	79	High	NNE–SSW
Xizhoushan	50	Crystalline basement	320	0.36	72	High	NE–SW
Shilingguan	5	Low-grade metasediments	217	0.4	57	High	NE–SW
Jiaocheng	48	Low-grade metasediments	193	0.32	39	Low	NE–SW
Taigu	49	Low-grade metasediments	168	0.29	33	Low	NE–SW
Huoshan	12	Crystalline basement	301	0.36	68	High	NE–SW
Luoyunshan	38	Low-grade metasediments and crystalline basement	219	0.38	47	Medium	E–W
Zhongtiaoshan	72	Crystalline basement	208	0.31	43	Medium	NNE–SSW

5.2 Implications for rift evolution, linkage, and seismic hazard

Two significant zones in the evolution of the Shanxi Rift are the Shilingguan and Lingshi RIZs, which formed between the major basins. Both zones are generally more elevated than the surrounding basins, making them potential sediment sources (Gawthorpe and Leeder, 2000). This is also evidenced by their patchy, thin sediment fill compared to that of the major basins (Xu and Ma, 1992). The two RIZs differ in their geometrical organisation. The Shilingguan RIZ can be described as an underlapping, parallel, divergent RIZ, while the Lingshi RIZ is an underlapping, oblique, convergent RIZ – see Fig. 3 in Kolawole et al. (2021a) for comparison. A potential third RIZ, the Hengshan RIZ, which separates the Datong and Xinding basins, can be proposed (Fig. 2). However, as it is an overlapping, divergent RIZ, it is completely unbreached; therefore, it will not be discussed at length in the following. The different RIZ stages come with distinct morphological responses and have implications for the seismic hazard; thus, in the following, we classify the two RIZs in the Shanxi Rift based on the Kolawole et al. (2021a) classification scheme and assess the response of the geomorphic indices.

The Lingshi RIZ (Fig. 8) is the uplifted region between the Taiyuan and Linfen basins. The breaching fault, which in this case is the Huoshan fault, is well developed and has established a physical connection between the Taiyuan and Linfen basins. The Huoshan fault and other small-scale faults within the Lingshi RIZ are shorter, more segmented, and variably oriented compared to the faults of the major subbasins. These small-scale faults are more visible in the slope map (Fig. 8c) as sharp linear breaks. The footwall of the Huoshan fault shows high HI values, greater than 0.5 (Fig. 8b). However, the entire RIZ shows high HI values, which are sometimes connected to smaller-scale faults, highlighting the complexity and distribution of faulting in the RIZ. As noted in Sect. 5.1, the Loess Plateau can have a significant impact on the HI response of a region; therefore, the high HI response in the Lingshi RIZ may partly be related to the degree of loess coverage. However, the loess is constrained to the hanging wall of the Huoshan fault, and, therefore, the high HI response in the Huoshan fault footwall is not influenced by loess. The drainage of the Taiyuan and Linfen basins is connected across the Lingshi RIZ as the Fen River flows through it. The drainage was previously not connected due to possible paleodrainage divides (shown in purple in Fig. 8a), where tributaries of streams flowed in separate directions. Li et al. (1998) proposed that during the early evolution of the Shanxi Rift in the Miocene and Pliocene, the basins were filled by isolated lakes, and later, during the mid-Pleistocene, a fluvial connection was established. Hu et al. (2005) identified three lake terraces in the Taiyuan and Linfen basins, with the latest regression occurring at 0.13 Ma. Based on this, the integration and breaching across the Lingshi RIZ likely occurred in the mid-Pleistocene to Late Pleistocene. The swath profile of the RIZ and the longitudinal river profile (Fig. 8d and e) show a down-stepping morphology that is commonly associated with recently breached RIZs; this may be a relic of the lake terraces that existed prior the establishment of the fluvial connection. The Huoshan breaching fault is well developed and has established a physical connection between the depositional systems of both basins. Given the charac-

teristic morphology of the Lingshi RIZ, we classify it as a recently breached RIZ.

The Shilingguan RIZ (Fig. 9) separates the Xinding Basin to the north and the Taiyuan Basin to the south. The breaching fault (i.e. the Shilingguan fault) is physically connected to the Jiaocheng fault but not to the Xizhoushan fault. The Shilingguan fault appears to be segmented, as demonstrated by the various orientations of the fault segments (Fig. 9c). The topographic swath profile of the RIZ shows an outstanding topographic high (Fig. 9d). The footwall of the Shilingguan fault exhibits very high (> 0.5) HI values, and the Fen River in its footwall is highly sinuous but has a high topography, a high relief, and steep slopes on both sides, forming an entrenched meander (Gardner, 1975; Harden, 1990). Combining all these observations indicates that this area of the Shanxi Rift has experienced recent uplift. The Shilingguan RIZ represents a drainage divide, with the Hutuo River, north of the RIZ, is being deflected eastwards and draining across the Xizhoushan fault through the Taihang Mountains into the North China Plain (Fig. 2). In contrast, the Fen River flows from the northwest, crossing the main breaching fault before draining southwards into the Taiyuan basin. Wind gaps (Fig. 9a) in the footwall of the Xizhoushan fault to the east suggest that the drainage of the upper part of the Fen River may have previously occurred across this RIZ from west to east, prior to the initiation of the Shilingguan fault and the uplift of its footwall, which caused the diversion of the river to the south. As the depositional systems of the Xinding and Taiyuan basins are not connected across the RIZ (and the breaching fault has not established a full physical link), this RIZ represents a partially breached RIZ.

The different breaching stages of the Lingshi and Shilingguan RIZs may be related to their previously mentioned geometrical arrangements (the Lingshi RIZ is an underlapping, oblique, convergent RIZ, whereas the Shilingguan RIZ is an underlapping, parallel, divergent RIZ), which led to the earlier breaching of the Lingshi RIZ. The influence of the initial geometry was demonstrated by Kolawole et al. (2024) in a numerical model of the southern Malawi Rift, where the tip-to-tip arrangement of the Nsanje RIZ favoured rift coalescence more than the overlapping, divergent geometry of the Middle Shire RIZ. The convergent RIZ geometry of the Lingshi RIZ was beneficial for strain localisation and stress concentration at the fault tips of the surrounding basin-bounding faults (i.e. the Jiaocheng and Linfen faults), while the divergent geometry of the Shilingguan RIZ stalled rift coalescence. This, in turn, may also explain why the Hengshan RIZ is unbreached as its overlapping, divergent geometry is unfavourable for stress concentration and rift coalescence. The breaching status of the RIZs increases towards the south, which may be controlled by the different RIZ geometries.

Geomorphic evidence shows that the RIZs are currently the most active regions of faulting and reorganisation as breaching faults in the RIZs (i.e. the Huoshan and Shilingguan faults) show consistently high geomorphic values (Table 1; Fig. 7). They also show major changes in fault strike compared to the NE–SW-trending basins (Figs. 8 and 9). Most faults in the RIZs do not strike NE–SW but show more distributed patterns of N–S-striking and NE–SW-striking faults. Commonly, an overall zigzag pattern forms, with fault segments exhibiting variable direction. Faults oblique to the general extension direction commonly form at the intersection points between major faults (Figs. 2, 8, and 9). Hodge et al. (2018a) showed in models that Coulomb stress changes along the tips of established faults lead to the formation of new off-axis-trending faults, with the geometry of these faults dependent on lateral separation and the amount of underlap or overlap with the interacting faults. This process is common in other rift basins across the world (Maerten, 2000; Morley, 2010) and is similar to that observed in faults located in the RIZs of Shanxi. The N–S-striking fault segments in the RIZs show overall higher geomorphic-index values compared to the NE–SW-trending faults of the sub-basins, suggesting that they are more tectonically active as the active deformation is focused along zones of active linkage. The morphology of the N–S faults in the RIZs suggests that they are younger faults, still early in the reorganisation phase, as they are shorter and more segmented and often show a lower topographic offset (Figs. 8 and 9). NE–SW-striking basin-bounding faults that are more morphologically mature have lower geomorphic-index values than the faults in the RIZs but can still show high values, which is especially the case for the Wutai and Xizhoushan faults (Figs. 5 and 7). In the Shanxi Rift, faults of all orientations may show high activity levels; however, faults in the RIZs show the highest activity. This activity pattern is consistent with an overall stable extension direction (Middleton et al., 2017), where all faults remain potentially active but the activity is concentrated in the linkage zones.

RIZs often experience high seismic activity due to increased strain along the tips of established basin-bounding faults that progressively link across the RIZs. This was observed at the tips of the Rukwa rift and the Rukwa–Tanganyika RIZ by Kolawole et al. (2021a) and Kolawole et al. (2024), as well as in the Turkana rift (Musila et al., 2023). The breaching faults in the RIZ could have a buffering effect on the NE–SW-trending faults of the main sub-basins as the overall strain accommodated across the Shanxi Rift is concentrated on the breaching faults in the RIZs; therefore, the longer NE–SW-trending faults accommodate less strain overall. Increased strain rates on faults following linkage have been shown to occur both in theoretical frameworks (Cowie et al., 2005) and in natural examples, such as the Whakatāne Graben, New Zealand (Taylor et al., 2004). The heightened activity in these RIZs is evidenced not only by geomorphology but also by seismicity: Chen et al. (2021) processed receiver function data showing clusters of earthquakes in or near the Lingshi and Shilingguan RIZs, whereas events in the individual sub-basins have been shown to be more distributed. The ISC catalogue (Storchak et al., 2013,

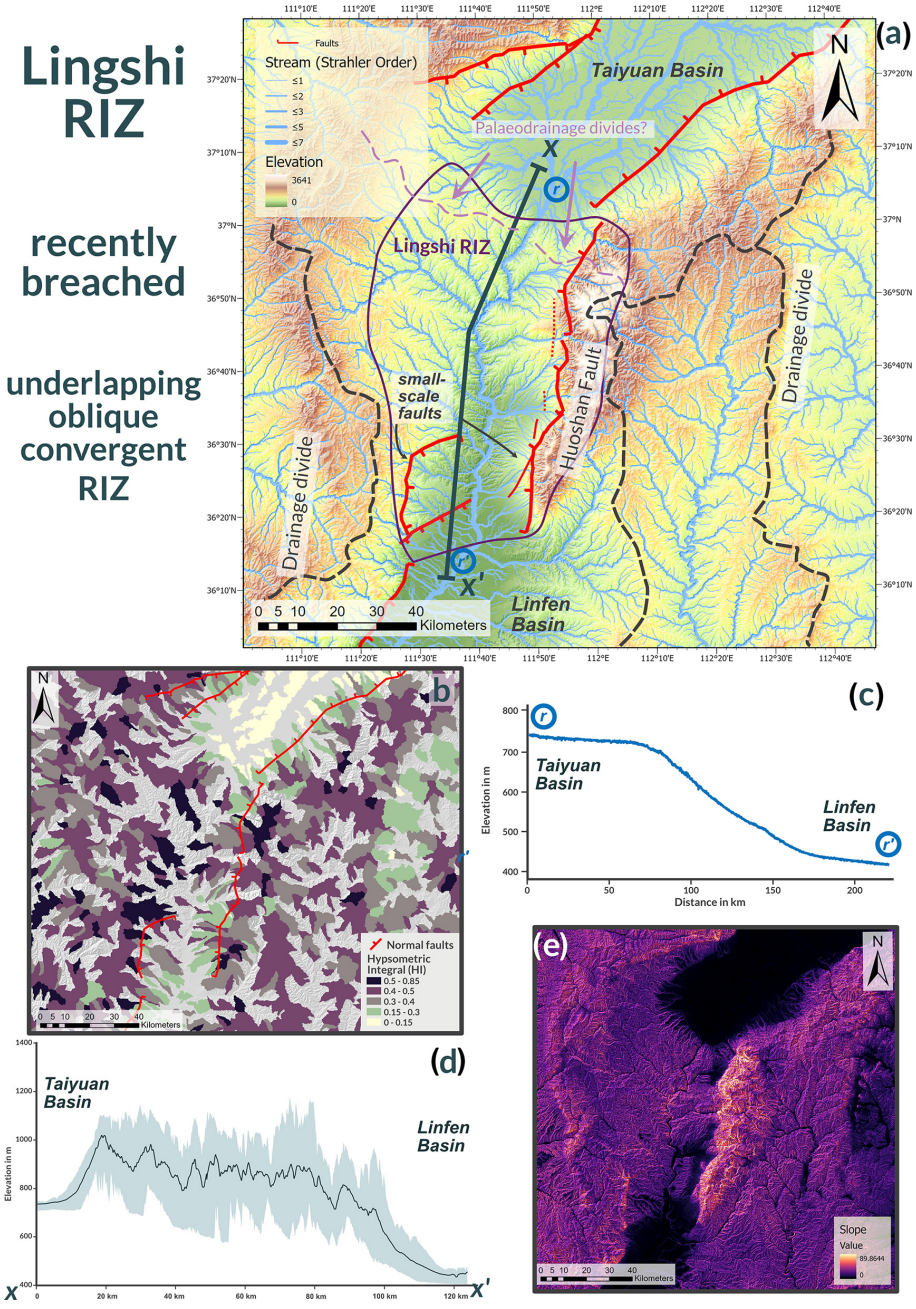

Figure 8. **(a)** Topographic map illustrating drainage (weighted by stream order). The map shows the drainage divide and reorganisation occurring in the Lingshi RIZ. **(b)** HI map of the Lingshi RIZ showing high values not only for the footwall of the Huoshan fault but also for the hanging wall. **(c)** Longitudinal river profile of the upper part of the Fen River, showing the characteristic "down-stepping" shape of river profiles across recently breached RIZs. **(d)** Swath profile of the Lingshi RIZ; the shaded area indicates maximum and minimum elevations in a 5 km corridor along the line of the section, shown in panel **(a)**. **(e)** Slope map of the Lingshi RIZ, which not only shows very high values along the main border fault (Huoshan) but also shows clear distinct breaks in the SW.

2015; Di Giacomo et al., 2018), covering earthquakes occurring between 1907 and 2022 (Fig. 2), shows similar clusters around the RIZs, although the cluster around the Shilingguan RIZ is more pronounced. The faults in the Shilingguan RIZ are comparatively short and segmented (10–20 km), which might limit the occurrence of large-magnitude earthquakes along their trace. However, the Huoshan fault, the breaching fault of the Lingshi RIZ, is equally segmented (Fig. 7a), with segments that are 20–30 km in length, and it has been the site of major historic earthquakes. The historic Hongdong earthquake (M_w 7.2–7.6) in 1303 was caused by slip on the Huoshan fault (Xu et al., 2018) and had an estimated rupture

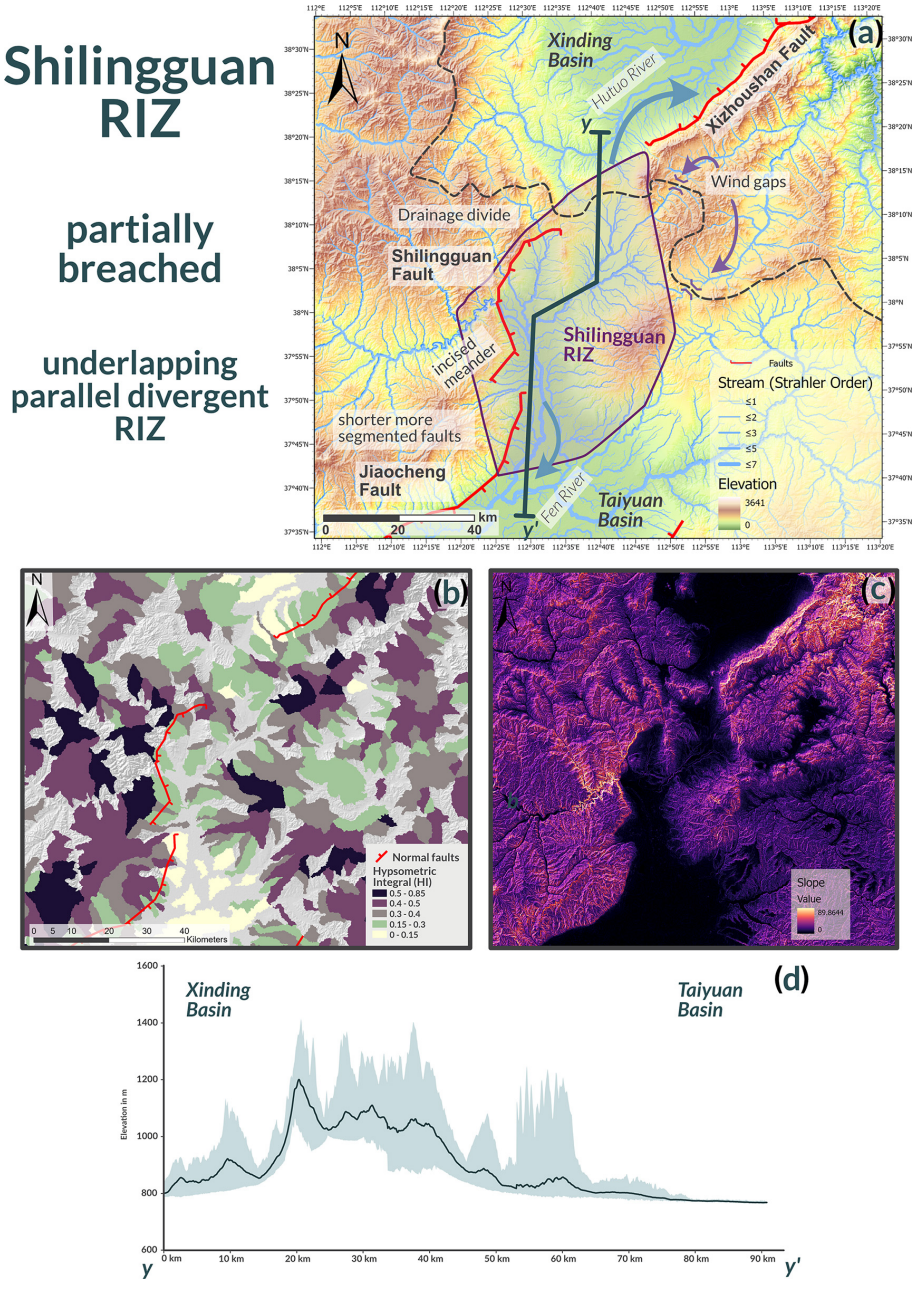

Figure 9. **(a)** Topographic map illustrating streams (weighted by stream order). The map shows the drainage divide and reorganisation occurring in the Shilingguan RIZ. **(b)** HI map of the Shilingguan RIZ showing high values for the footwalls of the main faults, especially the footwall of the Shilingguan fault, where high slope values are found. **(c)** Slope map of the Shilingguan RIZ. High slope values are closely associated with the main faults and can also be seen along the steep sides of meandering rivers with respect to the footwalls of the Xizhoushan fault and the Shilingguan fault. **(d)** Swath profile of the Shilingguan RIZ; shaded area indicates maximum and minimum elevations in a 5 km corridor along the line of the section, shown in panel **(a)**.

length of 98 km, which shows that multiple segments can link up during seismic slip to generate larger-magnitude events. The Shanxi Rift is a low-strain-rate region, meaning major earthquakes are infrequent but potentially devastating, as evidenced by the 1303 Hongdong earthquake (Xu et al., 2018). Overall, the NE–SW-trending faults, which are longer but potentially less active, might be capable of generating larger but less frequent events (Scholz, 1982; Leonard, 2010), while the more segmented faults in the RIZs could produce more frequent earthquakes that are smaller in magnitude.

5.3 The role of inheritance in the Shanxi Rift – crust or mantle control?

Most continental rifts are influenced by inherited structures that are reactivated (Daly et al., 1989; Wheeler and Karson, 1989; Holdsworth et al., 2001; Kinabo et al., 2008; Phillips et al., 2016; Wedmore et al., 2020; Kolawole et al., 2021b) or by those that reorient the rift-scale strain field in local areas (Morley, 2010; Philippon et al., 2015; Kolawole et al., 2018; Samsu et al., 2023). The Shanxi Rift exploited rheological weaknesses during its formation at the rift scale (TNCO) and on smaller individual fault scales. At first order, the spatial relationship between the Shanxi Rift and the TNCO is obvious (Fig. 1). The Shanxi Rift is directly superimposed onto the Paleoproterozoic orogen (Xu et al., 1993). The TNCO served as a rheological weakness in comparison to the stronger, adjacent Western Block of the NCC, and, therefore, the TNCO was exploited by the Shanxi Rift. Orogenic belts acting as weak zones for nucleating rifts is a common feature of, for example, the East African Rift (Rosendahl, 1987; Morley, 1988; Daly et al., 1989; Ring, 1994) and the Baikal Rift (Petit et al., 1996). In the Shanxi Rift, faults often define the edges of Paleoproterozoic basement complexes and expose these at the surface through footwall uplift (e.g. the Wutai, Hengshan, Xizhoushan, and Zhongtiaoshan faults). In some of the rift faults, footwalls do not contain Precambrian crystalline rocks, but, for example, the Jiaocheng and Taigu faults, located in the direct vicinity of the crystalline Lüliang and Taihang massifs ($\sim$ 50 km distance), do contain such rocks. Basement complexes, such as the Huoshan, Fuping, and Lüliang complexes, are also cored by Precambrian granitic plutons, which formed as late orogenic intrusions during the development of the TNCO. These stronger, more buoyant granitic blocks may have been more resistant to deformation, leading the rift faults to preferentially form along the pluton margins and be uplifted within the fault footwall. This finding is similar to observations from offshore New Zealand (Phillips and McCaffrey, 2019; Phillips et al., 2023) or Carboniferous rift systems in the United Kingdom (Fraser and Gawthorpe, 1990; Howell et al., 2020).

The similar trends regarding ancient pre-existing structures and active extensional faults show that the Paleoproterozoic fabrics of the TNCO potentially influence the orientation of the active faults in the Shanxi Graben. Major NE–SW-trending basin-bounding faults in the Shanxi Rift (i.e. the Wutai, Xizhoushan, Taigu, Jiaocheng, and Zhongtiaoshan faults) are generally parallel to inherited NE–SW-trending (45–55°) Paleoproterozoic basement fabrics (Fig. 4). The Wutai and Zhongtiaoshan faults both strike ENE–WSW (60–70°), aligning with the trend of the inherited structures in the footwall (Fig. 4). Therefore, it is likely that crustal structures influenced the orientation of these faults. The Hengshan fault locally trends parallel to the basement fabrics but often strikes obliquely and cuts across some of the shallow basement fabrics observed at surface (Fig. 4). It is possible that this fault locally exploits shallow basement fabrics while following the trend of a deeper-seated weakness that is oblique to the shallow basement fabrics observed at surface, similar to the behaviour of the Bilila–Mtakataka fault (Hodge et al., 2018b) in Malawi. The Xizhoushan fault follows the trend of the fabrics in the western part of the Fuping Complex. There is a major crustal boundary running through the Fuping Complex, known as the Longquanguan thrust (LGQT), which, according to Trap et al. (2012), is a gently dipping thrust fault. Southeast of the LGQT, there is a major change in the trend of the Paleoproterozoic fabrics to a generally NW–SE/E–W direction (compare the stereonets of "Fuping-West" and "Fuping-East" shown in Fig. 4). The crustal structures of the eastern part of the Fuping Block have no influence on the Xizhoushan fault (or any other fault in the Shanxi Rift), possibly because the LGQT represents a mechanical barrier. Based on their proximity and matching orientation, we speculate that the Xizhoushan fault may merge with the LGQT at depth. The merging of faults on shallower-dipping structures has been observed by Phillips et al. (2016) in the North Sea. The $>$ 50 km long basin-bounding faults of the Shanxi Rift nucleated along preferentially orientated inherited fabrics of the Paleoproterozoic basement complexes, which may have aided early fault nucleation, similar to observations in other global rift systems (Phillips et al., 2016; Rotevatn et al., 2018; Heilman et al., 2019; Collanega et al., 2019; Vasconcelos et al., 2019; Ramos et al., 2022)

Faults in the RIZs show a more disconnected pattern (Figs. 8 and 9), vary more in orientation (N–S and NE–SW), and are shorter (10–30 km) compared to the large NE–SW-trending basin-bounding faults (up to 100 km). Individual fault segments in the RIZs follow the broadly NE–SW-trending inherited crustal fabric or cut across the fabric, striking N–S or NNE–SSW. As RIZ faults mature, segments link up and grow into one throughgoing zigzag structure that cuts across pre-existing fabrics. This is especially visible in the plan view of the Huoshan fault (Fig. 8). These zigzag patterns in faults have been observed in offshore West Greenland (Peace et al., 2018; Schiffer et al., 2020), the North Sea (Henza et al., 2011; Henstra et al., 2015), and the Main Ethiopian Rift (Moore and Davidson, 1978; Vetel and Le Gall, 2006; Corti et al., 2022; Lezzar et al., 2002; Corti, 2009; Hodge et al., 2018b). In the cases of Greenland and Ethiopia, rifting was oblique to major basement shear zones, which led to the formation of two sets of faults, with some faults parallel to the extension direction and others parallel to the inherited structures. In the Shanxi Rift, the regional NW–SE extensional vector (Middleton et al., 2017) is likely perturbed around the RIZs due to interactions among the fault tips of adjacent basin-bounding faults, resulting in a strain field that is oblique to the inherited structures. This leads to the formation of N–S-trending faults that are perpendicular to the perturbed strain field and cut across the inherited basement fabrics, as well as NE–SW-trending faults that follow the trend of pre-existing Proterozoic structures. Therefore, as the faults

grow and coalesce across the RIZs, they cut across or locally exploit the inherited fabrics (Heilman et al., 2019; Kolawole et al., 2021b), resulting in the observed zigzag fault pattern. Fault geometry may also be controlled by multiple levels of inheritance, as noted by Wedmore et al. (2020) for the Thyolo fault in Malawi and by Hodge et al. (2018b) for the Bilila–Mtakataka fault, where shallow-level structures control the surface geometry of the fault, while a deeper-seated weakness guides the overall orientation, which is oblique to the overall strain field. We propose that the NE–SW-trending faults in the RIZs initially formed parallel to inherited fabrics and were later linked by N–S-trending segments. This behaviour was observed at the Norwegian margin of the North Sea by Henstra et al. (2015), where rift faults from an early phase of rifting influenced the location and morphology of younger rift faults during a subsequent oblique phase of rifting. However, we did not find major morphological or geomorphological value differences between the N–S-trending and NE–SW-trending faults that would suggest a polyphase fault development; therefore, it is possible that they are coeval.

The N–S-trending and NE–SW-trending faults in the RIZs can also be observed at the scale of the entire Shanxi Rift. The Shanxi Rift is an S-shaped en echelon rift that follows a broad N–S trend, with individual basins and their bounding faults oriented NE–SW. While the TNCO broadly trends N–S/NNE–SSW (Fig. 1; Zhao et al., 2005), individual crustal structures (such as major shear zones, thrust faults, and fabrics) broadly trend NE–SW (Fig. 10). Anisotropy that broadly trends from NNE–SSW to N–S (0–15°) in the upper mantle of the central zone of the North China Craton is indicated by shear-wave-splitting data from the upper mantle (Chen, 2010; Zhao and Zheng, 2005). The apparent obliquity between the trend of crustal structures and the upper-mantle fabric shows that crustal inheritance and lithospheric inheritance may not share a common orientation, which is a common feature of many rift zones (Vauchez et al., 1997; Tommasi and Vauchez, 2001). Recent analogue modelling of oblique crustal and mantle fabrics by Zwaan et al. (2022) shows patterns similar to those observed in the Shanxi Rift. Analogue models by Molnar et al. (2020) show that lithospheric weaknesses influence the rift trend, while oblique crustal structures segment the rift on a local scale. The difference in lithospheric and crustal structural trends could have occurred during the transpressional accretion of the TNCO, as proposed by Li et al. (2010), where subduction initially occurred along an N–S trend, with a later collision forming NE–SW-trending structures. Alternatively, the polyorogenic event that formed the TNCO may have formed the obliquity between crustal and mantle structures as the initial N–S-trending TNCO was partially reworked by a collision with the supercontinent Columbia in the Paleoproterozoic (Kusky and Li, 2003; Kusky et al., 2007; Santosh, 2010). However, the evolutionary history of the TNCO is debated, and resolving the exact timing of these events is beyond the scope of this paper. Mesozoic compression across northern China, commonly known as the Yanshanian orogeny (Zhang et al., 2008, 2011; Clinkscales and Kapp, 2019), has also affected the Shanxi region and may have also caused further reworking of the TNCO, rotating the crustal fabrics to their present-day orientation. The apparent obliquity between crustal and lithospheric trends of the TNCO is not resolvable in this study and would require further work on the kinematic evolution of the TNCO. The principal extension direction of 151° for the Shanxi Rift, determined by Middleton et al. (2017), is roughly perpendicular to the inherited crustal structures but oblique to the proposed broad upper-mantle anisotropy, resulting in early rift basins exploiting the favourably orientated crustal fabrics, while the general trend of the rift is oblique to the extension direction along an upper-mantle fabric, creating a rheological weakness. This en echelon arrangement of rift basins above a broad, oblique, deep-seated weak zone has been observed in analogue models by Agostini et al. (2009), which show similar geometries to those exhibited by the Shanxi Rift. However, we acknowledge that the observed mantle anisotropy may not be an inherited mantle fabric and could have formed during rifting (Gao et al., 1997; Kendall et al., 2006), aligning obliquely to the rift (Tepp et al., 2018; Ebinger et al., 2024). Thus, the mantle fabric underlying Shanxi may be Cenozoic in age and could have formed during the extensional deformation of northern China, as previously proposed (Chang et al., 2012). We emphasise that our interpretation – that the architecture of the Shanxi Rift is influenced by crustal and mantle fabrics of the TNCO, which are oblique to each other – is speculative as the origin of the mantle anisotropy beneath the Shanxi Rift is unresolved. However, the apparent N–S trend of the TNCO, the roughly N–S-trending mantle anisotropy, and the NE–SW-trending crustal fabrics may support the hypothesis that the crust and mantle fabrics beneath the Shanxi Rift are oblique.

Based on our geomorphic results, we propose a new model for the evolution of the Shanxi Rift that incorporates a heterogeneous basement with inherited structures (Fig. 11). This model may explain the evolution of the Shanxi Rift under a constant and simpler strain field, rather than under a more variable strain field (Shi et al., 2015b, 2020; Assie et al., 2022). In our model, the extensional-strain field trends NW–SE, which is consistent with previous estimations of the present-day extensional-strain field using GPS or seismicity data (Middleton et al., 2017; Shen et al., 2000). However, locally, the strain is reoriented by inherited structures (i.e. the Wutai and Zhongtiaoshan faults; Figs. 5 and 8) or by interactions between basin-bounding faults that rotate the local strain field in the RIZs between them (i.e. the Shilingguan and Lingshi RIZs; Fig. 11). This means that there is no specific set of faults favoured by changes in strain fields. Therefore, potentially all faults remain active, but there are certain faults that are more active due to ongoing reorganisation and linkage in the RIZs. Faults were established during

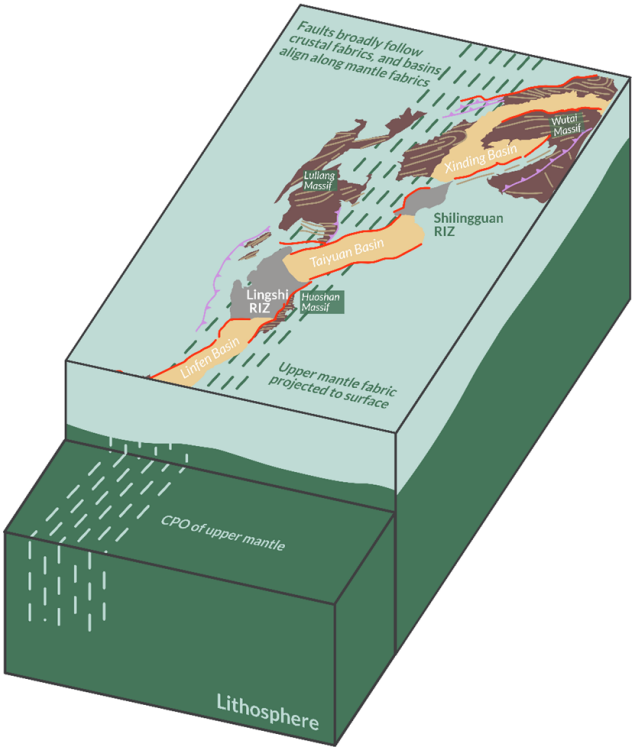

Figure 10. Schematic 3D diagram of the Shanxi Rift showing the proposed obliquity between mantle anisotropy and inherited crustal fabrics. Mantle anisotropy is defined by the suggested crystallographic preferred orientation (CPO) in the upper mantle, as evidenced by shear-wave-splitting data (Zhao and Zheng, 2005); the upper mantle broadly trends N–S, while the crustal fabrics trend NE–SW. The Shanxi Rift basins align with a zone of mantle fabric which is oblique to the principal extension direction (indicated by the purple arrows). Individual basins and their bounding faults formed parallel to inherited crustal fabrics, creating the characteristic en echelon pattern of the Shanxi Rift.

early evolutionary stages along preferentially aligned NE–SW-trending inherited structures and formed the major en echelon Taiyuan, Xinding, and Linfen basins along an N–S-trending upper-mantle structure (Figs. 10 and 11). As the faults and basins grew, they interacted and linked across almost unfaulted topographical high stands – the RIZs. These RIZs had a more complex faulting pattern as the interacting faults created a locally rotated strain field, oblique to the crustal structures and the regional strain field. This created a zigzag geometry as the shorter fault segments grew and coalesced. As linkage progresses, these RIZs connect basins and establish physical and sedimentary system links. This linkage is currently ongoing, as demonstrated by the single partially breached RIZ in Shilingguan.

6 Conclusions

We applied three different geomorphic indices (R_l, k_{sn}, and the HI) to analyse the fault distribution and the geometry and occurrence of rift interaction zones (RIZs) along the Shanxi Rift. Our aims were to discuss the distribution of tectonic activity, understand the role that structural inheritance has played in its evolution, and discuss the seismic hazard posed by active faults within it. Based on our results, we conclude the following:

1. Geomorphic indices are a powerful tool for evaluating fault evolution, fault activity, and segmentation within the Shanxi Rift.

2. Our study shows that lithology has a strong influence on the overall geomorphic signal of faults as faults with Paleoproterozoic crystalline basement rocks in their footwalls exhibit higher geomorphic values compared to faults with Paleozoic–Mesozoic metasediments in their footwalls. However, comparing faults with similar basement geology can circumvent this problem. We found that, overall, the HI is less sensitive to these variations in lithology compared to local relief and k_{sn}. Therefore, the HI may be more suited for evaluating tectonic influences on landscapes.

3. Within the Shanxi Rift, the RIZs that link the well-developed Xinding, Linfen, and Taiyuan basins are the most active zones and show the most signs of active drainage reorganisation. This has major implications for seismic-hazard assessments as it hints towards zones which show more complex and active faulting patterns due to strain concentration in the RIZs, leading to increased seismicity. Linkage of the basins seems to be progressing towards the north, as evidenced by the increasing breaching status of the RIZs towards the south, which is possibly controlled by their initial geometry.

4. Structural inheritance has played a key role in the evolution and segmentation of the Shanxi Rift. The collision of the two component blocks of the NCC created a lithospheric-scale weak zone, the Trans-North China Orogen (TNCO), which preferentially accommodates strain. The individual sub-basins of the Shanxi Rift form en echelon, aligning along a broad N–S trend that coincides with an upper-mantle anisotropy fabric – a lithospheric manifestation of the TNCO. The mantle anisotropy is oblique to the NW–SE extension direction, while the NE–SW-trending crustal fabrics are perpendicular to the extension direction. Early rift faults nucleated along NE–SW-oriented basement fabrics, establishing basins arranged along the inherited N–S trend. As the boundary faults grew, they began to interact and form RIZs. Within these RIZs, crustal basement inheritance further influenced and segmented the breaching

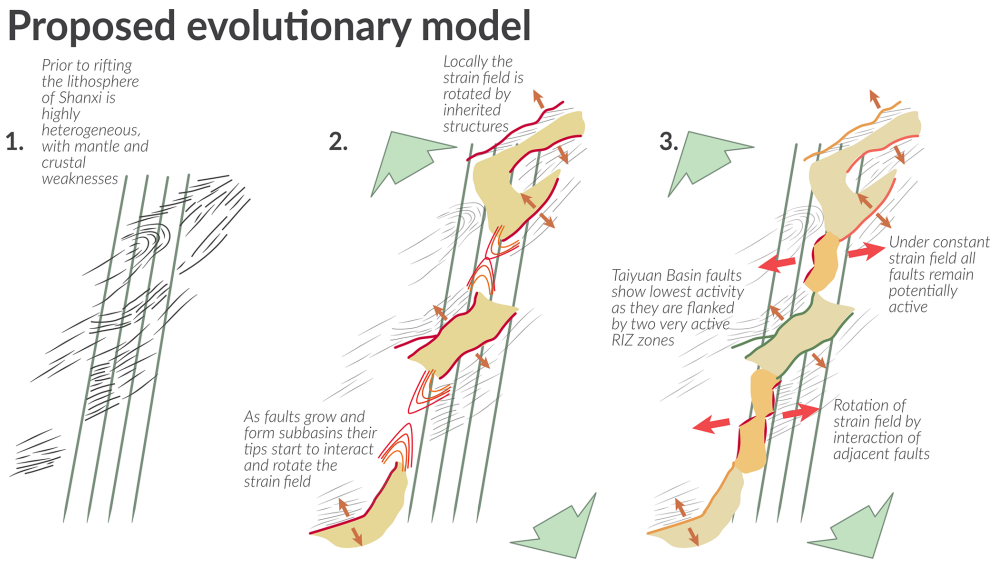

Figure 11. New proposed evolutionary model under a constant strain field showing the linkage of rift basins influenced by two levels of inheritance – crustal and mantle inheritance – which result in oblique rifting and the creation of an en echelon array of basins. (1) Proposed pre-rift framework of NNE–SSW-trending mantle fabrics and NE–SW-trending crustal fabrics. (2) Major basins form en echelon along the NNE–SSW-trending mantle fabric; however, they also form perpendicular to the extension direction (large green arrows) and along inherited crustal structures that locally reorient the strain (smaller orange arrows). RIZs are created, and major basin-bounding faults start to reorient the local strain field. (3) The RIZs are breached, forming smaller, more segmented fault segments that are influenced by the locally reoriented strain field (red arrows) and inherited crustal structures.

faults and aided linkage across the basins. The faults within the RIZs both follow and cross-cut pre-existing fabrics in the crust, creating a zigzag pattern of small, segmented faults that eventually link up into singular throughgoing fault zones. Therefore, the structural inheritance of pre-existing Precambrian basement fabrics and a locally rotated stress field resulted in the complex pattern of faulting observed in the RIZs.

5. Our geomorphic study supports a constant strain field during the formation of the Shanxi Rift, with minor changes in the extensional vector. We propose that the Shanxi Rift is a type example of an oblique rift, with its observed pattern of faulting influenced by postulated upper-mantle anisotropy, crustal basement fabrics, and pre-existing faults.

Code and data availability. A GeoPackage of the GIS project, including the associated raster files of the geomorphic indices, is available via the Zenodo repository associated with this publication at https://doi.org/10.5281/zenodo.10058450 (Froemchen et al., 2024a). These files can be opened with QGIS. The R code for calculating the hypsometric integral is available on GitHub at https://github.com/MFroemchen/R_Hypsometry (Froemchen et al., 2024b; https://doi.org/10.5281/zenodo.13794544, Froemchen, 2024).

Supplement. The supplement related to this article is available online at: https://doi.org/10.5194/se-15-1203-2024-supplement.

Author contributions. MF, KJWM, MBA, JvH, and TBP conceptualised the study. MF conducted the geomorphic and structural analyses. MF prepared the paper and figures, with input from KJWM, MBA, JvH, and all other co-authors. All co-authors contributed to writing, revising, and preparing the paper.

Competing interests. The contact author has declared that none of the authors has any competing interests.

Disclaimer. Publisher's note: Copernicus Publications remains neutral with regard to jurisdictional claims made in the text, published maps, institutional affiliations, or any other geographical representation in this paper. While Copernicus Publications makes every effort to include appropriate place names, the final responsibility lies with the authors.

Special issue statement. This article is part of the special issue "(D)rifting into the future: the relevance of rifts and divergent margins in the 21st century". It is not associated with a conference.

Financial support. This research has been supported by the Natural Environment Research Council (grant no. NE/S007431/1).

Review statement. This paper was edited by Patricia Cadenas Martínez and reviewed by Anindita Samsu, Folarin Kolawole, and Peng Su.

References

Aanyu, K. and Koehn, D.: Influence of pre-existing fabrics on fault kinematics and rift geometry of interacting segments: Analogue models based on the Albertine Rift (Uganda), Western Branch-East African Rift System, J. Afr. Earth Sci., 59, 168–184, https://doi.org/10.1016/j.jafrearsci.2010.10.003, 2011.

Agostini, A., Corti, G., Zeoli, A., and Mulugeta, G.: Evolution, pattern, and partitioning of deformation during oblique continental rifting: Inferences from lithospheric-scale centrifuge models, Geochem. Geophy. Geosy., 10, Q11015, https://doi.org/10.1029/2009GC002676, 2009.

Ahnert, F.: Functional relationships between denudation, relief, and uplift in large, mid-latitude drainage basins, Am. J. Sci., 268, 243–263, https://doi.org/10.2475/ajs.268.3.243, 1970.

Ai, S., Zheng, Y., He, L., and Song, M.: Joint inversion of ambient noise and earthquake data in the Trans-North China Orogen: On-going lithospheric modification and its impact on the Cenozoic continental rifting, Tectonophysics, 763, 73–85, https://doi.org/10.1016/j.tecto.2019.05.003, 2019.

Allen, M. B., Macdonald, D. I. M., Xun, Z., Vincent, S. J., and Brouet-Menzies, C.: Early Cenozoic two-phase extension and late Cenozoic thermal subsidence and inversion of the Bohai Basin, northern China, Mar. Petrol. Geol., 14, 951–972, https://doi.org/10.1016/S0264-8172(97)00027-5, 1997.

Assie, K. R., Wang, Y., Tranos, M. D., Ma, H., Kouamelan, K. S., Brantson, E. T., Zhou, L., and Ketchaya, Y. B.: Late Cenozoic faulting deformation of the Fanshi Basin (northern Shanxi rift, China), inferred from palaeostress analysis of mesoscale fault-slip data, Geol. Mag., 159, 2306–2322, https://doi.org/10.1017/S0016756822000085, 2022.

Brune, S., Corti, G., and Ranalli, G.: Controls of inherited lithospheric heterogeneity on rift linkage: Numerical and analog models of interaction between the Kenyan and Ethiopian rifts across the Turkana depression, Tectonics, 36, 1767–1786, https://doi.org/10.1002/2017TC004739, 2017.

Bull, W. B. and McFadden, L. D.: Tectonic Geomorphology North and South of the Garlock Fault, California, in: Geomorphology in Arid Regions, edited by: Doehring, D. O., Routledge, https://doi.org/10.4324/9780429299230, 1980.

Chang, L., Wang, C.-Y., and Ding, Z.: Upper mantle anisotropy beneath North China from shear wave splitting measurements, Tectonophysics, 522–523, 235–242, https://doi.org/10.1016/j.tecto.2011.12.009, 2012.

Chen, G.: On the geotectonic nature of the Fen-Wei rift system, Tectonophysics, 143, 217–223, https://doi.org/10.1016/0040-1951(87)90091-6, 1987.

Chen, L.: Concordant structural variations from the surface to the base of the upper mantle in the North China Craton and its tectonic implications, Lithos, 120, 96–115, https://doi.org/10.1016/j.lithos.2009.12.007, 2010.

Chen, W.-P. and Nábelek, J.: Seismogenic strike-slip faulting and the development of the North China Basin, Tectonics, 7, 975–989, https://doi.org/10.1029/TC007i005p00975, 1988.

Chen, Y., Chen, J., Li, S., Yu, Z., Liu, X., and Shen, X.: Variations of crustal thickness and average Vp/Vs ratio beneath the Shanxi Rift, North China, from receiver functions, Earth Planets Space, 73, 200, https://doi.org/10.1186/s40623-021-01528-8, 2021.

Chen, Y.-C., Sung, Q., and Cheng, K.-Y.: Along-strike variations of morphotectonic features in the Western Foothills of Taiwan: tectonic implications based on stream-gradient and hypsometric analysis, Geomorphology, 56, 109–137, https://doi.org/10.1016/S0169-555X(03)00059-X, 2003.

Clinkscales, C. and Kapp, P.: Structural style and kinematics of the Taihang-Luliangshan fold belt, North China: Implications for the Yanshanian orogeny, Lithosphere, 11, 767–783, https://doi.org/10.1130/L1096.1, 2019.

Clinkscales, C., Kapp, P., Thomson, S., Wang, H., Laskowski, A., Orme, D. A., and Pullen, A.: Regional exhumation and tectonic history of the Shanxi Rift and Taihangshan, North China, Tectonics, 40, e2020TC006416, https://doi.org/10.1029/2020TC006416, 2021.

Collanega, L., Siuda, K., A.-L. Jackson, C., Bell, R. E., Coleman, A. J., Lenhart, A., Magee, C., and Breda, A.: Normal fault growth influenced by basement fabrics: The importance of preferential nucleation from pre-existing structures, Basin Res., 31, 659–687, https://doi.org/10.1111/bre.12327, 2019.

Corti, G.: Continental rift evolution: From rift initiation to incipient break-up in the Main Ethiopian Rift, East Africa, Earth-Sci. Rev., 96, 1–53, https://doi.org/10.1016/j.earscirev.2009.06.005, 2009.

Corti, G., Iandelli, I., and Cerca, M.: Experimental modeling of rifting at craton margins, Geosphere, 9, 138–154, https://doi.org/10.1130/GES00863.1, 2013.

Corti, G., Maestrelli, D., and Sani, F.: Large-to Local-Scale Control of Pre-Existing Structures on Continental Rifting: Examples From the Main Ethiopian Rift, East Africa, Front. Earth Sci., 10, 808503, https://doi.org/10.3389/feart.2022.808503, 2022.

Cowie, P. A., Underhill, J. R., Behn, M. D., Lin, J., and Gill, C. E.: Spatio-temporal evolution of strain accumulation derived from multi-scale observations of Late Jurassic rifting in the northern North Sea: A critical test of models for lithospheric extension, Earth Planet. Sc. Lett., 234, 401–419, https://doi.org/10.1016/j.epsl.2005.01.039, 2005.

Cox, R. T.: Analysis of drainage-basin symmetry as a rapid technique to identify areas of possible Quaternary tilt-block tectonics: An example from the Mississippi Embayment, GSA Bulletin, 106, 571–581, https://doi.org/10.1130/0016-7606(1994)106<0571:AODBSA>2.3.CO;2, 1994.

Crider, J. G. and Pollard, D. D.: Fault linkage: Three-dimensional mechanical interaction between echelon normal faults, J. Geophys. Res.-Sol. Ea., 103, 24373–24391, https://doi.org/10.1029/98JB01353, 1998.

Daly, M. C., Chorowicz, J., and Fairhead, J. D.: Rift basin evolution in Africa: the influence of reactivated steep basement shear zones, Geological Society, London, Special Publications, 44, 309–334, https://doi.org/10.1144/GSL.SP.1989.044.01.17, 1989.

Davis, G., Zheng, Y., Cong, W., Darby, B., Zhang, C., and Gehrels, G.: Mesozoic tectonic evolution of the Yanshan fold and thrust belt, with emphasis on Hebei and Liaoning provinces, northern China, Geol. Soc. Am. Mem., 194, 171–197, https://doi.org/10.1130/0-8137-1194-0.171, 2001.

Deng, Q., Ran, Y., Yang, X., Min, W., and Chu, Q.: The active tectonic map of China (1 : 4 000 000), Seismological Press, ISBN 978-7-50-283051-9, 2007 (in Chinese).

Densmore, A. L., Dawers, N. H., Gupta, S., Allen, P. A., and Gilpin, R.: Landscape evolution at extensional relay zones, J. Geophys. Res.-Sol. Ea., 108, 2273, https://doi.org/10.1029/2001JB001741, 2003.

Densmore, A. L., Dawers, N. H., Gupta, S., Guidon, R., and Goldin, T.: Footwall topographic development during continental extension, J. Geophys. Res.-Earth, 109, F03001, https://doi.org/10.1029/2003JF000115, 2004.

Di Giacomo, D., Engdahl, E. R., and Storchak, D. A.: The ISC-GEM Earthquake Catalogue (1904–2014): status after the Extension Project, Earth Syst. Sci. Data, 10, 1877–1899, https://doi.org/10.5194/essd-10-1877-2018, 2018.

DiBiase, R. A., Whipple, K. X., Heimsath, A. M., and Ouimet, W. B.: Landscape form and millennial erosion rates in the San Gabriel Mountains, CA, Earth Planet. Sc. Lett., 289, 134–144, https://doi.org/10.1016/j.epsl.2009.10.036, 2010.

Dong, S., Zhang, Y., Zhang, F., Cui, J., Chen, X., Zhang, S., Miao, L., Li, J., Shi, W., Li, Z., Huang, S., and Li, H.: Late Jurassic–Early Cretaceous continental convergence and intracontinental orogenesis in East Asia: A synthesis of the Yanshan Revolution, J. Asian Earth Sci., 114, 750–770, https://doi.org/10.1016/j.jseaes.2015.08.011, 2015.

Dulanya, Z., Gallen, S. F., Kolawole, F., Williams, J. N., Wedmore, L. N. J., Biggs, J., and Fagereng, Å.: Knickpoint morphotectonics of the Middle Shire River basin: Implications for the evolution of rift interaction zones, Basin Res., 34, 1839–1858, https://doi.org/10.1111/bre.12687, 2022.

Dunbar, J. A. and Sawyer, D. S.: Continental rifting at pre-existing lithospheric weaknesses, Nature, 333, 450–452, https://doi.org/10.1038/333450a0, 1988.

Ebinger, C. J., Rosendahl, B. R., and Reynolds, D. J.: Tectonic model of the Malaŵi rift, Africa, Tectonophysics, 141, 215–235, https://doi.org/10.1016/0040-1951(87)90187-9, 1987.

Ebinger, C. J., Reiss, M. C., Bastow, I., and Karanja, M. M.: Shallow sources of upper mantle seismic anisotropy in East Africa, Earth Planet. Sc. Lett., 625, 118488, https://doi.org/10.1016/j.epsl.2023.118488, 2024.

Erbello, A., Melnick, D., Zeilinger, G., Bookhagen, B., Pingel, H., and Strecker, M. R.: Geomorphic expression of a tectonically active rift-transfer zone in southern Ethiopia, Geomorphology, 403, 108162, https://doi.org/10.1016/j.geomorph.2022.108162, 2022.

Farangitakis, G. P., Heron, P. J., McCaffrey, K. J. W., van Hunen, J., and Kalnins, L. M.: The impact of oblique inheritance and changes in relative plate motion on the development of rift-transform systems, Earth Planet. Sc. Lett., 541, 116277, https://doi.org/10.1016/j.epsl.2020.116277, 2020.

Faulds, J. E. and Varga, R. J.: The role of accommodation zones and transfer zones in the regional segmentation of extended terranes, in: Accommodation zones and transfer zones; the regional segmentation of the Basin and Range Province, vol. 323, edited by: Faulds, J. E. and Stewart, J. H., Geological Society of America, https://doi.org/10.1130/0-8137-2323-X.1, 1998.

Faure, M., Trap, P., Lin, W., Monié, P., and Bruguier, O.: Polyorogenic evolution of the Paleoproterozoic Trans-North China Belt – New insights from the Lüliangshan-Hengshan-Wutaishan and Fuping massifs, Episodes Journal of International Geoscience, 30, 96–107, 2007.

Fazlikhani, H., Fossen, H., Gawthorpe, R. L., Faleide, J. I., and Bell, R. E.: Basement structure and its influence on the structural configuration of the northern North Sea rift, Tectonics, 36, 1151–1177, https://doi.org/10.1002/2017TC004514, 2017.

Fernández-Blanco, D., de Gelder, G., Lacassin, R., and Armijo, R.: Geometry of Flexural Uplift by Continental Rifting in Corinth, Greece, Tectonics, 39, e2019TC005685, https://doi.org/10.1029/2019TC005685, 2020.

Fick, S. E. and Hijmans, R. J.: WorldClim 2: new 1 km spatial resolution climate surfaces for global land areas, Int. J. Climatol., 37, 4302–4315, https://doi.org/10.1002/joc.5086, 2017.

Fisher, J. A., Pazzaglia, F. J., Anastasio, D. J., and Gallen, S. F.: Linear Inversion of Fluvial Topography in the Northern Apennines: Comparison of Base-Level Fall to Crustal Shortening, Tectonics, 41, e2022TC007379, https://doi.org/10.1029/2022TC007379, 2022.

Flint, J.-J.: Stream gradient as a function of order, magnitude, and discharge, Water Resour. Res., 10, 969–973, 1974.

Fossen, H. and Rotevatn, A.: Fault linkage and relay structures in extensional settings – A review, Earth-Sci. Rev., 154, 14–28, https://doi.org/10.1016/j.earscirev.2015.11.014, 2016.

Fraser, A. J. and Gawthorpe, R. L.: Tectono-stratigraphic development and hydrocarbon habitat of the Carboniferous in northern England, Geological Society, London, Special Publications, 55, 49–86, https://doi.org/10.1144/GSL.SP.1990.055.01.03, 1990.

Froemchen, M.: MFroemchen/R_Hypsometry: R_Hypsometry_1.0 (v.1.0), Zenodo [code], https://doi.org/10.5281/zenodo.13794544, 2024.

Froemchen, M., McCaffrey, K., Allen, M., van Hunen, J., Phillips, T., and Yueren, X.: Geomorphic expressions of active rifting reflect the role of structural inheritance: A new model for the evolution of the Shanxi Rift, North China, Zenodo [data set], https://doi.org/10.5281/zenodo.10058450, 2024a.

Froemchen, M., McCaffrey, K., Allen, M., van Hunen, J., Phillips, T., and Yueren, X.: R_Hypsometry, GitHub [code], https://github.com/MFroemchen/R_Hypsometry, last access: 15 September 2024b.

Gallen, S. F. and Fernández-Blanco, D.: A New Data-Driven Bayesian Inversion of Fluvial Topography Clarifies the Tectonic History of the Corinth Rift and Reveals a Channel Steepness Threshold, J. Geophys. Res.-Earth, 126, e2020JF005651, https://doi.org/10.1029/2020JF005651, 2021.

Gao, M., Zeilinger, G., Xu, X., Tan, X., Wang, Q., and Hao, M.: Active tectonics evaluation from geomorphic indices for the central and the southern Longmenshan range on the Eastern Tibetan Plateau, China, Tectonics, 35, 1812–1826, https://doi.org/10.1002/2015TC004080, 2016.

Gao, S., Davis, P. M., Liu, H., Slack, P. D., Rigor, A. W., Zorin, Y. A., Mordvinova, V. V., Kozhevnikov, V. M., and Logatchev, N. A.: SKS splitting beneath continental rift zones, J. Geophys. Res.-Sol. Ea., 102, 22781–22797, https://doi.org/10.1029/97JB01858, 1997.

Gao, S., Rudnick, R. L., Carlson, R. W., McDonough, W. F., and Liu, Y.-S.: Re–Os evidence for replacement of ancient mantle lithosphere beneath the North China craton, Earth Planet. Sc. Lett., 198, 307–322, https://doi.org/10.1016/S0012-821X(02)00489-2, 2002.

Gao, S., Rudnick, R. L., Yuan, H.-L., Liu, X.-M., Liu, Y.-S., Xu, W.-L., Ling, W.-L., Ayers, J., Wang, X.-C., and Wang, Q.-H.: Recycling lower continental crust in the North China craton, Nature, 432, 892–897, https://doi.org/10.1038/nature03162, 2004.

Gardner, T. W.: The History of Part of the Colorado River and Its Tributaries: An Experimental Study, Four Corners Geol. Soc. Guidebook, Canyonlands, 87–95, 1975.

Gawthorpe, R. L. and Hurst, J. M.: Transfer zones in extensional basins: their structural style and influence on drainage development and stratigraphy, Journal of the Geological Society, 150, 1137–1152, https://doi.org/10.1144/gsjgs.150.6.1137, 1993.

Gawthorpe, R. L. and Leeder, M. R.: Tectono-sedimentary evolution of active extensional basins, Basin Res., 12, 195–218, https://doi.org/10.1111/j.1365-2117.2000.00121.x, 2000.

Geurts, A. H., Whittaker, A. C., Gawthorpe, R. L., and Cowie, P. A.: Transient landscape and stratigraphic responses to drainage integration in the actively extending central Italian Apennines, Geomorphology, 353, 107013, https://doi.org/10.1016/j.geomorph.2019.107013, 2020.

Goldsworthy, M. and Jackson, J.: Active normal fault evolution in Greece revealed by geomorphology and drainage patterns, Journal of the Geological Society, 157, 967–981, https://doi.org/10.1144/jgs.157.5.967, 2000.

Griffin, W. L., Andi, Z., O'Reilly, S. Y., and Ryan, C. G.: Phanerozoic Evolution of the Lithosphere Beneath the Sino-Korean Craton, in: Mantle Dynamics and Plate Interactions in East Asia, edited by: Flower, M. F. J., Chung, S.-L., Lo, C.-H., and Lee, T.-Y., American Geophysical Union (AGU), 107–126, ISBN 978-1-118-67013-2, https://agupubs.onlinelibrary.wiley.com/doi/10.1029/GD027p0107 (last access: 18 September 2024), 1998.

Groves, K., Saville, C., Hurst, M. D., Jones, S. J., Song, S., and Allen, M. B.: Geomorphic expressions of collisional tectonics in the Qilian Shan, north eastern Tibetan Plateau, Tectonophysics, 788, 228503, https://doi.org/10.1016/j.tecto.2020.228503, 2020.

Hack, J. T.: Studies of longitudinal stream profiles in Virginia and Maryland, Professional Paper, USGS, https://doi.org/10.3133/pp294B, 1957.

Hamdouni, R., Irigaray, C., Castillo, T., Chacón, J., and Keller, E.: Assessment of relative active tectonics, southwest border of the Sierra Nevada (southern Spain), Geomorphology, 96, 150–173, https://doi.org/10.1016/j.geomorph.2007.08.004, 2008.

Harden, D. R.: Controlling factors in the distribution and development of incised meanders in the central Colorado Plateau, GSA Bulletin, 102, 233–242, https://doi.org/10.1130/0016-7606(1990)102<0233:CFITDA>2.3.CO;2, 1990.

He, J., Liu, M., and Li, Y.: Is the Shanxi rift of northern China extending?, Geophys. Res. Lett., 30, 2213, https://doi.org/10.1029/2003GL018764, 2003.

Heilman, E., Kolawole, F., Atekwana, E. A., and Mayle, M.: Controls of Basement Fabric on the Linkage of Rift Segments, Tectonics, 38, 1337–1366, https://doi.org/10.1029/2018TC005362, 2019.

Henstra, G. A., Rotevatn, A., Gawthorpe, R. L., and Ravnås, R.: Evolution of a major segmented normal fault during multiphase rifting: The origin of plan-view zigzag geometry, J. Struct. Geol., 74, 45–63, https://doi.org/10.1016/j.jsg.2015.02.005, 2015.

Henza, A. A., Withjack, M. O., and Schlische, R. W.: How do the properties of a pre-existing normal-fault population influence fault development during a subsequent phase of extension?, J. Struct. Geol., 33, 1312–1324, https://doi.org/10.1016/j.jsg.2011.06.010, 2011.

Heron, P. J., Peace, A. L., McCaffrey, K. J. W., Welford, J. K., Wilson, R., van Hunen, J., and Pysklywec, R. N.: Segmentation of Rifts Through Structural Inheritance: Creation of the Davis Strait, Tectonics, 38, 2411–2430, https://doi.org/10.1029/2019TC005578, 2019.

Hodge, M., Fagereng, Å., Biggs, J., and Mdala, H.: Controls on early-rift geometry: New perspectives from the Bilila-Mtakataka Fault, Malawi, Geophys. Res. Lett., 45, 3896–3905, 2018a.

Hodge, M., Fagereng, Å., and Biggs, J.: The Role of Coseismic Coulomb Stress Changes in Shaping the Hard Link Between Normal Fault Segments, J. Geophys. Res.-Sol. Ea., 123, 797–814, https://doi.org/10.1002/2017JB014927, 2018b.

Holdsworth, R. E., Stewart, M., Imber, J., and Strachan, R. A.: The structure and rheological evolution of reactivated continental fault zones: a review and case study, Geological Society, London, Special Publications, 184, 115–137, https://doi.org/10.1144/GSL.SP.2001.184.01.07, 2001.

Howell, L., Egan, S., Leslie, G., Clarke, S., Mitten, A., and Pringle, J.: The influence of low-density granite bodies on extensional basins, Geology Today, 36, 22–26, https://doi.org/10.1111/gto.12297, 2020.

Hu, X., Li, Y., and Yang, J.: Quaternary paleolake development in the Fen River basin, North China, Geomorphology, 65, 1–13, https://doi.org/10.1016/j.geomorph.2004.06.008, 2005.

Hurtrez, J.-E., Sol, C., and Lucazeau, F.: Effect of drainage area on hypsometry from an analysis of small-scale drainage basins in the Siwalik Hills (Central Nepal), Earth Surf. Proc. Land., 24, 799–808, https://doi.org/10.1002/(SICI)1096-9837(199908)24:9<799::AID-ESP12>3.0.CO;2-4, 1999.

Jackson, J. and Leeder, M.: Drainage systems and the development of normal faults: an example from Pleasant Valley, Nevada, J. Struct. Geol., 16, 1041–1059, https://doi.org/10.1016/0191-8141(94)90051-5, 1994.

Kapp, P., Pullen, A., Pelletier, J. D., Russell, J., Goodman, P., and Cai, F.: From dust to dust: Quaternary wind erosion of the Mu Us Desert and Loess Plateau, China, Geology, 43, 835–838, https://doi.org/10.1130/G36724.1, 2015.

Kattenhorn, S. A., Aydin, A., and Pollard, D. D.: Joints at high angles to normal fault strike: an explanation using 3-D numerical models of fault-perturbed stress fields, J. Struct. Geol., 22, 1–23, https://doi.org/10.1016/S0191-8141(99)00130-3, 2000.

Kendall, J.-M., Pilidou, S., Keir, D., Bastow, I. D., Stuart, G. W., and Ayele, A.: Mantle upwellings, melt migration and the rifting of Africa: insights from seismic anisotropy, Geological Society, London, Special Publications, 259, 55–72, https://doi.org/10.1144/GSL.SP.2006.259.01.06, 2006.

Kinabo, B. D., Hogan, J. P., Atekwana, E. A., Abdelsalam, M. G., and Modisi, M. P.: Fault growth and propagation during incipient continental rifting: Insights from a combined aeromagnetic and Shuttle Radar Topography Mission digital elevation model investigation of the Okavango Rift Zone, northwest Botswana, Tectonics, 27, TC3013, https://doi.org/10.1029/2007TC002154, 2008.

Kirby, E. and Whipple, K. X.: Expression of active tectonics in erosional landscapes, J. Struct. Geol., 44, 54–75, https://doi.org/10.1016/j.jsg.2012.07.009, 2012.

Koehn, D., Aanyu, K., Haines, S., and Sachau, T.: Rift nucleation, rift propagation and the creation of basement microplates within active rifts, Tectonophysics, 458, 105–116, https://doi.org/10.1016/j.tecto.2007.10.003, 2008.

Kolawole, F., Atekwana, E. A., Laó-Dávila, D. A., Abdelsalam, M. G., Chindandali, P. R., Salima, J., and Kalindekafe, L.: Active deformation of Malawi rift's north basin Hinge zone modulated by reactivation of preexisting Precambrian Shear zone fabric, Tectonics, 37, 683–704, 2018.

Kolawole, F., Firkins, M. C., Al Wahaibi, T. S., Atekwana, E. A., and Soreghan, M. J.: Rift interaction zones and the stages of rift linkage in active segmented continental rift systems, Basin Res., 33, 2984–3020, 2021a.

Kolawole, F., Phillips, T. B., Atekwana, E. A., and Jackson, C. A.-L.: Structural Inheritance Controls Strain Distribution During Early Continental Rifting, Rukwa Rift, Front. Earth Sci., 9, 707869, https://doi.org/10.3389/feart.2021.707869, 2021b.

Kolawole, F., Vick, T., Atekwana, E. A., Laó-Dávila, D. A., Costa, A. G., and Carpenter, B. M.: Strain localization and migration during the pulsed lateral propagation of the Shire Rift Zone, East Africa, Tectonophysics, 839, 229499, https://doi.org/10.1016/j.tecto.2022.229499, 2022.

Kolawole, F., Xue, L., and Dulanya, Z.: Rapid Versus Delayed Linkage and Coalescence of Propagating Rift Tips, ESS Open Archive, https://doi.org/10.22541/essoar.168167202.29986035/v2, 4 March 2024.

Krabbendam, M. and Barr, T. D.: Proterozoic orogens and the break-up of Gondwana: why did some orogens not rift?, J. Afr. Earth Sci., 31, 35–49, https://doi.org/10.1016/S0899-5362(00)00071-3, 2000.

Kusky, T. M. and Li, J.: Paleoproterozoic tectonic evolution of the North China Craton, J. Asian Earth Sci., 22, 383–397, https://doi.org/10.1016/S1367-9120(03)00071-3, 2003.

Kusky, T., Li, J., and Santosh, M.: The Paleoproterozoic North Hebei Orogen: North China craton's collisional suture with the Columbia supercontinent, Gondwana Res., 12, 4–28, https://doi.org/10.1016/j.gr.2006.11.012, 2007.

Lambiase, J. J. and Bosworth, W.: Structural controls on sedimentation in continental rifts, Geological Society, London, Special Publications, 80, 117–144, https://doi.org/10.1144/GSL.SP.1995.080.01.06, 1995.

Leeder, M. R. and Jackson, J. A.: The interaction between normal faulting and drainage in active extensional basins, with examples from the western United States and central Greece, Basin Res., 5, 79–102, https://doi.org/10.1111/j.1365-2117.1993.tb00059.x, 1993.

Leonard, M.: Earthquake Fault Scaling: Self-Consistent Relating of Rupture Length, Width, Average Displacement, and Moment Release, B. Seismol. Soc. Am., 100, 1971–1988, https://doi.org/10.1785/0120090189, 2010.

Lezzar, K. E., Tiercelin, J.-J., Le Turdu, C., Cohen, Andrew. S., Reynolds, D. J., Le Gall, B., and Scholz, C. A.: Control of Normal Fault Interaction on the Distribution of Major Neogene Sedimentary Depocenters, Lake Tanganyika, East African Rift, AAPG Bull., 86, 1027–1059, https://doi.org/10.1306/61EEDC1A-173E-11D7-8645000102C1865D, 2002.

Li, S., Zhao, G., Wilde, S. A., Zhang, J., Sun, M., Zhang, G., and Dai, L.: Deformation history of the Hengshan–Wutai–Fuping Complexes: Implications for the evolution of the Trans-North China Orogen, Gondwana Res., 18, 611–631, https://doi.org/10.1016/j.gr.2010.03.003, 2010.

Li, Y., Yang, J., Xia, Z., and Mo, D.: Tectonic geomorphology in the Shanxi Graben System, northern China, Geomorphology, 23, 77–89, https://doi.org/10.1016/S0169-555X(97)00092-5, 1998.

Lifton, N. A. and Chase, C. G.: Tectonic, climatic and lithologic influences on landscape fractal dimension and hypsometry: implications for landscape evolution in the San Gabriel Mountains, California, Geomorphology, 5, 77–114, https://doi.org/10.1016/0169-555X(92)90059-W, 1992.

Maerten, L.: Variation in slip on intersecting normal faults: Implications for paleostress inversion, J. Geophys. Res.-Sol. Ea., 105, 25553–25565, https://doi.org/10.1029/2000JB900264, 2000.

Makrari, S., Sharma, G., Taloor, A. K., Singh, M. S., Sarma, K. K., and Aggarwal, S. P.: Assessment of the geomorphic indices in relation to tectonics along selected sectors of Borpani River Basin, Assam using Cartosat DEM data, Geosystems and Geoenvironment, 1, 100068, https://doi.org/10.1016/j.geogeo.2022.100068, 2022.

Masek, J. G., Isacks, B. L., Gubbels, T. L., and Fielding, E. J.: Erosion and tectonics at the margins of continental plateaus, J. Geophys. Res.-Sol. Ea., 99, 13941–13956, https://doi.org/10.1029/94JB00461, 1994.

McCaffrey, K. J. W.: Controls on reactivation of a major fault zone: the Fair Head–Clew Bay line in Ireland, Journal of the Geological Society, 154, 129–133, https://doi.org/10.1144/gsjgs.154.1.0129, 1997.

Menzies, M. A. and Xu, Y.: Geodynamics of the North China Craton, in: Mantle Dynamics and Plate Interactions in East Asia, edited by: Flower, M. F. J., Chung, S.-L., Lo, C.-H., and Lee, T.-Y., American Geophysical Union (AGU), 155–165, https://agupubs.onlinelibrary.wiley.com/doi/abs/10.1029/GD027p0155 (last access: 18 September 2024), 1998.

Menzies, M., Xu, Y., Zhang, H., and Fan, W.: Integration of geology, geophysics and geochemistry: A key to understanding the North China Craton, Lithos, 96, 1–21, https://doi.org/10.1016/j.lithos.2006.09.008, 2007.

Menzies, M. A., Fan, W., and Zhang, M.: Palaeozoic and Cenozoic lithoprobes and the loss of >120 km of Archaean lithosphere, Sino-Korean craton, China, Geological Society, London, Special Publications, 76, 71–81, https://doi.org/10.1144/GSL.SP.1993.076.01.04, 1993.

Middleton, T. A., Elliott, J. R., Rhodes, E. J., Sherlock, S., Walker, R. T., Wang, W., Yu, J., and Zhou, Y.: Extension rates across the northern Shanxi Grabens, China, from Quaternary geology, seismicity and geodesy, Geophys. J. Int., 209, 535–558, 2017.

Molnar, N., Cruden, A., and Betts, P.: The role of inherited crustal and lithospheric architecture during the evolution of the Red Sea: Insights from three dimensional analogue experiments, Earth Planet. Sc. Lett., 544, 116377, https://doi.org/10.1016/j.epsl.2020.116377, 2020.

Moore, J. M. and Davidson, A.: Rift structure in southern Ethiopia, Tectonophysics, 46, 159–173, https://doi.org/10.1016/0040-1951(78)90111-7, 1978.

Morley, C. K.: Variable extension in Lake Tanganyika, Tectonics, 7, 785–801, https://doi.org/10.1029/TC007i004p00785, 1988.

Morley, C. K.: Stress re-orientation along zones of weak fabrics in rifts: An explanation for pure extension in "oblique" rift segments?, Earth Planet. Sc. Lett., 297, 667–673, https://doi.org/10.1016/j.epsl.2010.07.022, 2010.

Morley, C. K., Nelson, R. A., Patton, T. L., and Munn, S. G.: Transfer Zones in the East African Rift System and Their Relevance to Hydrocarbon Exploration in Rifts (1), AAPG Bull., 74, 1234–1253, https://doi.org/10.1306/0C9B2475-1710-11D7-8645000102C1865D, 1990.

Morley, C. K., Haranya, C., Phoosongsee, W., Pongwapee, S., Kornsawan, A., and Wonganan, N.: Activation of rift oblique and rift parallel pre-existing fabrics during extension and their effect on deformation style: examples from the rifts of Thailand, J. Struct. Geol., 26, 1803–1829, https://doi.org/10.1016/j.jsg.2004.02.014, 2004.

Mulaya, E., Gluyas, J., McCaffrey, K., Phillips, T., and Ballentine, C.: Structural geometry and evolution of the Rukwa Rift Basin, Tanzania: Implications for helium potential, Basin Res., 34, 938–960, https://doi.org/10.1111/bre.12646, 2022.

Musila, M., Ebinger, C. J., Bastow, I. D., Sullivan, G., Oliva, S. J., Knappe, E., Perry, M., Kounoudis, R., Ogden, C. S., Bendick, R., Mwangi, S., Mariita, N., Kianji, G., Kraus, E., and Illsley-Kemp, F.: Active Deformation Constraints on the Nubia-Somalia Plate Boundary Through Heterogenous Lithosphere of the Turkana Depression, Geochem. Geophy. Geosy., 24, e2023GC010982, https://doi.org/10.1029/2023GC010982, 2023.

Nelson, R. A., Patton, T. L., and Morley, C. K.: Rift-Segment Interaction and Its Relation to Hydrocarbon Exploration in Continental Rift Systems (1), AAPG Bull., 76, 1153–1169, 1992.

Obaid, A. K. and Allen, M. B.: Landscape expressions of tectonics in the Zagros fold-and-thrust belt, Tectonophysics, 766, 20–30, https://doi.org/10.1016/j.tecto.2019.05.024, 2019.

Osagiede, E. E., Rotevatn, A., Gawthorpe, R., Kristensen, T. B., Jackson, C. A.-L., and Marsh, N.: Pre-existing intra-basement shear zones influence growth and geometry of non-colinear normal faults, western Utsira High–Heimdal Terrace, North Sea, J. Struct. Geol., 130, 103908, https://doi.org/10.1016/j.jsg.2019.103908, 2020.

Pavlides, S. B., Zouros, N. C., Zhongjing, F., Shaoping, C., Tranos, M. D., and Chatzipetros, A. A.: Geometry, kinematics and morphotectonics of the Yanqing–Huailai active faults (northern China), Tectonophysics, 308, 99–118, https://doi.org/10.1016/S0040-1951(99)00074-8, 1999.

Peace, A., McCaffrey, K., Imber, J., van Hunen, J., Hobbs, R., and Wilson, R.: The role of pre-existing structures during rifting, continental breakup and transform system development, offshore West Greenland, Basin Res., 30, 373–394, https://doi.org/10.1111/bre.12257, 2018.

Pérez-Peña, J. V., Azañón, J. M., Booth-Rea, G., Azor, A., and Delgado, J.: Differentiating geology and tectonics using a spatial autocorrelation technique for the hypsometric integral, J. Geophys. Res.-Earth, 114, F02018, https://doi.org/10.1029/2008JF001092, 2009.

Perron, J. T. and Royden, L.: An integral approach to bedrock river profile analysis, Earth Surf. Proc. Land., 38, 570–576, https://doi.org/10.1002/esp.3302, 2013.

Petit, C., Deverchere, J., Houdry, F., Sankov, V. A., Melnikova, V. I., and Delvaux, D.: Present-day stress field changes along the Baikal rift and tectonic implications, Tectonics, 15, 1171–1191, 1996.

Philippon, M., Willingshofer, E., Sokoutis, D., Corti, G., Sani, F., Bonini, M., and Cloetingh, S.: Slip re-orientation in oblique rifts, Geology, 43, 147–150, 2015.

Phillips, T. B. and McCaffrey, K. J. W.: Terrane Boundary Reactivation, Barriers to Lateral Fault Propagation and Reactivated Fabrics: Rifting Across the Median Batholith Zone, Great South Basin, New Zealand, Tectonics, 38, 4027–4053, https://doi.org/10.1029/2019TC005772, 2019.

Phillips, T. B., Jackson, C. A., Bell, R. E., Duffy, O. B., and Fossen, H.: Reactivation of intrabasement structures during rifting: A case study from offshore southern Norway, J. Struct. Geol., 91, 54–73, 2016.

Phillips, T. B., Naliboff, J. B., McCaffrey, K. J. W., Pan, S., van Hunen, J., and Froemchen, M.: The influence of crustal strength on rift geometry and development – insights from 3D numerical modelling, Solid Earth, 14, 369–388, https://doi.org/10.5194/se-14-369-2023, 2023.

Qi, J. and Yang, Q.: Cenozoic structural deformation and dynamic processes of the Bohai Bay basin province, China, Mar. Petrol. Geol., 27, 757–771, https://doi.org/10.1016/j.marpetgeo.2009.08.012, 2010.

Ramos, G. V., Vasconcelos, D. L., Marques, F. O., de Castro, D. L., Nogueira, F. C. C., Bezerra, F. H. R., Perez, Y. A. R., Souza, J. A. B., and Medeiros, V. C.: Relations between inherited basement fabric and fault nucleation in a continental setting: The Rio do Peixe Basin, NE Brazil, Mar. Petrol. Geol., 139, 105635, https://doi.org/10.1016/j.marpetgeo.2022.105635, 2022.

Reeve, M. T., Bell, R. E., Duffy, O. B., Jackson, C. A.-L., and Sansom, E.: The growth of non-colinear normal fault systems; What can we learn from 3D seismic reflection data?, J. Struct. Geol., 70, 141–155, 2015.

Ring, U.: The influence of preexisting structure on the evolution of the Cenozoic Malawi rift (East African rift system), Tectonics, 13, 313–326, https://doi.org/10.1029/93TC03188, 1994.

Rosendahl, B. R.: Architecture of Continental Rifts with Special Reference to East Africa, Annu. Rev. Earth Pl. Sc., 15, 445–503, https://doi.org/10.1146/annurev.ea.15.050187.002305, 1987.

Rotevatn, A., Kristensen, T. B., Ksienzyk, A. K., Wemmer, K., Henstra, G. A., Midtkandal, I., Grundvåg, S.-A., and Andresen, A.: Structural Inheritance and Rapid Rift-Length Establishment in a Multiphase Rift: The East Greenland Rift System and its Caledonian Orogenic Ancestry, Tectonics, 37, 1858–1875, https://doi.org/10.1029/2018TC005018, 2018.

Sachau, T., Koehn, D., Stamps, D. S., and Lindenfeld, M.: Fault kinematics and stress fields in the Rwenzori Mountains, Uganda, Int. J. Earth. Sci. (Geol. Rundsch.), 105, 1729–1740, https://doi.org/10.1007/s00531-015-1162-6, 2016.

Samsu, A., Cruden, A. R., Micklethwaite, S., Grose, L., and Vollgger, S. A.: Scale matters: The influence of structural inheritance on fracture patterns, J. Struct. Geol., 130, 103896, https://doi.org/10.1016/j.jsg.2019.103896, 2020.

Samsu, A., Micklethwaite, S., Williams, J. N., Fagereng, Å., and Cruden, A. R.: Structural inheritance in amagmatic rift basins: Manifestations and mechanisms for how pre-existing struc-

tures influence rift-related faults, Earth-Sci. Rev., 246, 104568, https://doi.org/10.1016/j.earscirev.2023.104568, 2023.

Santosh, M.: Assembling North China Craton within the Columbia supercontinent: The role of double-sided subduction, Precambrian Res., 178, 149–167, https://doi.org/10.1016/j.precamres.2010.02.003, 2010.

Schiffer, C., Doré, A. G., Foulger, G. R., Franke, D., Geoffroy, L., Gernigon, L., Holdsworth, B., Kusznir, N., Lundin, E., McCaffrey, K., Peace, A. L., Petersen, K. D., Phillips, T. B., Stephenson, R., Stoker, M. S., and Welford, J. K.: Structural inheritance in the North Atlantic, Earth-Sci. Rev., 206, 102975, https://doi.org/10.1016/j.earscirev.2019.102975, 2020.

Schmidt, K. M. and Montgomery, D. R.: Limits to Relief, Science, 270, 617–620, https://doi.org/10.1126/science.270.5236.617, 1995.

Scholz, C. A.: Deltas of the Lake Malawi Rift, East Africa: Seismic Expression and Exploration Implications 1, AAPG Bull., 79, 1679–1697, https://doi.org/10.1306/7834DE54-1721-11D7-8645000102C1865D, 1995.

Scholz, C. H.: Scaling laws for large earthquakes: Consequences for physical models, B. Seismol. Soc. Am., 72, 1–14, 1982.

Schumacher, M. E.: Upper Rhine Graben: Role of preexisting structures during rift evolution, Tectonics, 21, 6-1–6-17, https://doi.org/10.1029/2001TC900022, 2002.

Schwanghart, W. and Scherler, D.: Short Communication: TopoToolbox 2 – MATLAB-based software for topographic analysis and modeling in Earth surface sciences, Earth Surf. Dynam., 2, 1–7, https://doi.org/10.5194/esurf-2-1-2014, 2014.

Şengör, A. M. C., Lom, N., and Sağdıç, N. G.: Tectonic inheritance, structure reactivation and lithospheric strength: the relevance of geological history, Geological Society, London, Special Publications, 470, 105–136, https://doi.org/10.1144/SP470.8, 2019.

Shanxi Bureau of Geology and Mineral Resources (SBGMR): Regional Geology of Shanxi Province, Geological Publishing House, Beijing, China, 1989.

Shen, Z.-K., Zhao, C., Yin, A., Li, Y., Jackson, D. D., Fang, P., and Dong, D.: Contemporary crustal deformation in east Asia constrained by Global Positioning System measurements, J. Geophys. Res.-Sol. Ea., 105, 5721–5734, https://doi.org/10.1029/1999JB900391, 2000.

Shi, W., Cen, M., Chen, L., Wang, Y., Chen, X., Li, J., and Chen, P.: Evolution of the late Cenozoic tectonic stress regime in the Shanxi Rift, central North China Plate inferred from new fault kinematic analysis, J. Asian Earth Sci., 114, 54–72, https://doi.org/10.1016/j.jseaes.2015.04.044, 2015a.

Shi, W., Dong, S., Liu, Y., Hu, J., Chen, X., and Chen, P.: Cenozoic tectonic evolution of the South Ningxia region, northeastern Tibetan Plateau inferred from new structural investigations and fault kinematic analyses, Tectonophysics, 649, 139–164, https://doi.org/10.1016/j.tecto.2015.02.024, 2015b.

Shi, W., Dong, S., and Hu, J.: Neotectonics around the Ordos Block, North China: A review and new insights, Earth-Sci. Rev., 200, 102969, https://doi.org/10.1016/j.earscirev.2019.102969, 2020.

Snyder, N. P., Whipple, K. X., Tucker, G. E., and Merritts, D. J.: Landscape response to tectonic forcing: Digital elevation model analysis of stream profiles in the Mendocino triple junction region, northern California, Geol. Soc. Am. Bull., 112, 1250–1263, 2000.

Storchak, D. A., Di Giacomo, D., Bondar, I., Engdahl, E. R., Harris, J., Lee, W. H. K., Villasenor, A., and Bormann, P.: Public Release of the ISC-GEM Global Instrumental Earthquake Catalogue (1900–2009), Seismol. Res. Lett., 84, 810–815, https://doi.org/10.1785/0220130034, 2013.

Storchak, D. A., Di Giacomo, D., Engdahl, E. R., Harris, J., Bondár, I., Lee, W. H., Bormann, P., and Villaseñor, A.: The ISC-GEM global instrumental earthquake catalogue (1900–2009): introduction, Phys. Earth Planet. In., 239, 48–63, 2015.

Strahler, A. N.: Hypsometirc (area-altitude) Analysis of erosional topography, GSA Bulletin, 63, 1117–1142, https://doi.org/10.1130/0016-7606(1952)63[1117:HAAOET]2.0.CO;2, 1952.

Strahler, A. N.: Quantitative analysis of watershed geomorphology, Eos T. Am. Geophys. Un., 38, 913–920, https://doi.org/10.1029/TR038i006p00913, 1957.

Su, P., He, H., Tan, X., Liu, Y., Shi, F., and Kirby, E.: Initiation and evolution of the Shanxi Rift System in North China: Evidence from low-temperature thermochronology in a plate reconstruction framework, Tectonics, 40, e2020TC006298, https://doi.org/10.1029/2020TC006298, 2021.

Su, P., He, H., Liu, Y., Shi, F., Granger, D. E., Kirby, E., Luo, L., Han, F., and Lu, R.: Quantifying the Structure and Extension Rate of the Linfen Basin, Shanxi Rift System Since the Latest Miocene: Implications for Continental Magma-Poor Rifting, Tectonics, 42, e2023TC007885, https://doi.org/10.1029/2023TC007885, 2023.

Tang, Y.-C., Fen, Y.-G., Chen Zhongshun, J., Zhou, S.-Y., Ning, J.-Y., Wei, S.-Q., Li, P., Chun-Quan, Y., Fan, W.-Y., and Wang, H.-Y.: Receiver function analysis at Shanxi Rift, Chinese Journal of Geophysics, 53, 2102–2109, https://doi.org/10.3969/j.issn.0001-5733.2010.09.010, 2010.

Taylor, S. K., Bull, J. M., Lamarche, G., and Barnes, P. M.: Normal fault growth and linkage in the Whakatane Graben, New Zealand, during the last 1.3 Myr, J. Geophys. Res.-Sol. Ea., 109, B02408, https://doi.org/10.1029/2003JB002412, 2004.

Tepp, G., Ebinger, C. J., Zal, H., Gallacher, R., Accardo, N., Shillington, D. J., Gaherty, J., Keir, D., Nyblade, A. A., Mbogoni, G. J., Chindandali, P. R. N., Ferdinand-Wambura, R., Mulibo, G. D., and Kamihanda, G.: Seismic Anisotropy of the Upper Mantle Below the Western Rift, East Africa, J. Geophys. Res.-Sol. Ea., 123, 5644–5660, https://doi.org/10.1029/2017JB015409, 2018.

Tommasi, A. and Vauchez, A.: Continental rifting parallel to ancient collisional belts: an effect of the mechanical anisotropy of the lithospheric mantle, Earth Planet. Sc. Lett., 185, 199–210, https://doi.org/10.1016/S0012-821X(00)00350-2, 2001.

Trap, P., Faure, M., Lin, W., and Monié, P.: Late Paleoproterozoic (1900–1800 Ma) nappe stacking and polyphase deformation in the Hengshan–Wutaishan area: Implications for the understanding of the Trans-North-China Belt, North China Craton, Precambrian Res., 156, 85–106, https://doi.org/10.1016/j.precamres.2007.03.001, 2007.

Trap, P., Faure, M., Lin, W., Bruguier, O., and Monié, P.: Contrasted tectonic styles for the Paleoproterozoic evolution of the North China Craton. Evidence for a $\sim$ 2.1 Ga thermal and tectonic event in the Fuping Massif, J. Struct. Geol., 30, 1109–1125, https://doi.org/10.1016/j.jsg.2008.05.001, 2008.

Trap, P., Faure, M., Lin, W., and Meffre, S.: The Lüliang Massif: a key area for the understanding of the Palaeoproterozoic Trans-

North China Belt, North China Craton, Geological Society, London, Special Publications, 323, 99–125, 2009a.

Trap, P., Faure, M., Lin, W., Monié, P., Meffre, S., and Melleton, J.: The Zanhuang Massif, the second and eastern suture zone of the Paleoproterozoic Trans-North China Orogen, Precambrian Res., 172, 80–98, 2009b.

Trap, P., Faure, M., Lin, W., Le Breton, N., and Monié, P.: Paleoproterozoic tectonic evolution of the Trans-North China Orogen: Toward a comprehensive model, Precambrian Res., 222–223, 191–211, https://doi.org/10.1016/j.precamres.2011.09.008, 2012.

Vasconcelos, D. L., Bezerra, F. H. R., Medeiros, W. E., de Castro, D. L., Clausen, O. R., Vital, H., and Oliveira, R. G.: Basement fabric controls rift nucleation and postrift basin inversion in the continental margin of NE Brazil, Tectonophysics, 751, 23–40, https://doi.org/10.1016/j.tecto.2018.12.019, 2019.

Vauchez, A., Barruol, G., and Tommasi, A.: Why do continents break-up parallel to ancient orogenic belts?, Terra Nova, 9, 62–66, https://doi.org/10.1111/j.1365-3121.1997.tb00003.x, 1997.

Versfelt, J. and Rosendahl, B. R.: Relationships between pre-rift structure and rift architecture in Lakes Tanganyika and Malawi, East Africa, Nature, 337, 354–357, https://doi.org/10.1038/337354a0, 1989.

Vetel, W. and Le Gall, B.: Dynamics of prolonged continental extension in magmatic rifts: the Turkana Rift case study (North Kenya), Geological Society, London, Special Publications, 259, 209–233, https://doi.org/10.1144/GSL.SP.2006.259.01.17, 2006.

Walcott, R. C. and Summerfield, M. A.: Scale dependence of hypsometric integrals: An analysis of southeast African basins, Geomorphology, 96, 174–186, https://doi.org/10.1016/j.geomorph.2007.08.001, 2008.

Wedmore, L. N. J., Williams, J. N., Biggs, J., Fagereng, Å., Mphepo, F., Dulanya, Z., Willoughby, J., Mdala, H., and Adams, B. A.: Structural inheritance and border fault reactivation during active early-stage rifting along the Thyolo fault, Malawi, J. Struct. Geol., 139, 104097, https://doi.org/10.1016/j.jsg.2020.104097, 2020.

Wedmore, L. N. J., Turner, T., Biggs, J., Williams, J. N., Sichingabula, H. M., Kabumbu, C., and Banda, K.: The Luangwa Rift Active Fault Database and fault reactivation along the southwestern branch of the East African Rift, Solid Earth, 13, 1731–1753, https://doi.org/10.5194/se-13-1731-2022, 2022.

Wheeler, W. H. and Karson, J. A.: Structure and kinematics of the Livingstone Mountains border fault zone, Nyasa (Malawi) Rift, southwestern Tanzania, Journal of African Earth Sciences (and the Middle East), 8, 393–413, https://doi.org/10.1016/S0899-5362(89)80034-X, 1989.

Whipple, K. X.: Bedrock rivers and the geomorphology of active orogens, Annu. Rev. Earth Pl. Sc., 32, 151–185, https://doi.org/10.1146/annurev.earth.32.101802.120356, 2004.

Whittaker, A. C.: How do landscapes record tectonics and climate?, Lithosphere, 4, 160–164, 2012.

Whittaker, A. C. and Walker, A. S.: Geomorphic constraints on fault throw rates and linkage times: Examples from the Northern Gulf of Evia, Greece, J. Geophys. Res.-Earth, 120, 137–158, https://doi.org/10.1002/2014JF003318, 2015.

Whittaker, A. C., Attal, M., Cowie, P. A., Tucker, G. E., and Roberts, G.: Decoding temporal and spatial patterns of fault uplift using transient river long profiles, Geomorphology, 100, 506–526, https://doi.org/10.1016/j.geomorph.2008.01.018, 2008.

Wilson, J. T.: Did the Atlantic Close and then Re-Open?, Nature, 211, 676–681, https://doi.org/10.1038/211676a0, 1966.

Wilson, R. W., Holdsworth, R. E., Wild, L. E., McCaffrey, K. J. W., England, R. W., Imber, J., and Strachan, R. A.: Basement-influenced rifting and basin development: a reappraisal of post-Caledonian faulting patterns from the North Coast Transfer Zone, Scotland, Geological Society, London, Special Publications, 335, 795–826, https://doi.org/10.1144/SP335.32, 2010.

Wobus, C., Whipple, K. X., Kirby, E., Snyder, N., Johnson, J., Spyropolou, K., Crosby, B., and Sheehan, D.: Tectonics from topography: Procedures, promise, and pitfalls, in: Tectonics, Climate, and Landscape Evolution, vol. 398, edited by: Willett, S. D., Hovius, N., Brandon, M. T., and Fisher, D. M., Geological Society of America, https://doi.org/10.1130/2006.2398(04), 2006.

Wong, W. H.: Crustal Movements and Igneous Activities in Eastern China Since Mesozoic Time, Bulletin of the Geological Society of China, 6, 9–37, https://doi.org/10.1111/j.1755-6724.1927.mp6001002.x, 1927.

Xu, X. and Ma, X.: Geodynamics of the Shanxi rift system, China, Tectonophysics, 208, 325–340, 1992.

Xu, X., Ma, X., and Deng, Q.: Neotectonic activity along the Shanxi rift system, China, Tectonophysics, 219, 305–325, 1993.

Xu, Y., He, H., Deng, Q., Allen, M. B., Sun, H., and Bi, L.: The CE 1303 Hongdong Earthquake and the Huoshan Piedmont Fault, Shanxi Graben: Implications for Magnitude Limits of Normal Fault Earthquakes, J. Geophys. Res.-Sol. Ea., 123, 3098–3121, https://doi.org/10.1002/2017JB014928, 2018.

Yin, A.: Cenozoic tectonic evolution of Asia: A preliminary synthesis, Tectonophysics, 488, 293–325, https://doi.org/10.1016/j.tecto.2009.06.002, 2010.

Zhai, M., Li, T.-S., Peng, P., Hu, B., Liu, F., and Zhang, Y.: Precambrian key tectonic events and evolution of the North China craton, Geological Society, London, Special Publications, 338, 235–262, https://doi.org/10.1144/SP338.12, 2010.

Zhai, M.-G. and Santosh, M.: The early Precambrian odyssey of the North China Craton: A synoptic overview, Gondwana Res., 20, 6–25, https://doi.org/10.1016/j.gr.2011.02.005, 2011.

Zhang, C., Li, C., Deng, H., Liu, Y., Liu, L., Wei, B., Li, H., and Liu, Z.: Mesozoic contraction deformation in the Yanshan and northern Taihang mountains and its implications to the destruction of the North China Craton, Sci. China Earth Sci., 54, 798–822, https://doi.org/10.1007/s11430-011-4180-7, 2011.

Zhang, Y., Ma, Y., Yang, N., Shi, W., and Dong, S.: Cenozoic extensional stress evolution in North China, J. Geodyn., 36, 591–613, https://doi.org/10.1016/j.jog.2003.08.001, 2003.

Zhang, Y., Dong, S., Zhao, Y., and Zhang, T.: Jurassic Tectonics of North China: A Synthetic View, Acta Geol. Sin.-Engl., 82, 310–326, https://doi.org/10.1111/j.1755-6724.2008.tb00581.x, 2008.

Zhang, Y. Q., Mercier, J. L., and Vergély, P.: Extension in the graben systems around the Ordos (China), and its contribution to the extrusion tectonics of south China with respect to Gobi-Mongolia, Tectonophysics, 285, 41–75, https://doi.org/10.1016/S0040-1951(97)00170-4, 1998.

Zhao, G., Min, S., Wilde, S. A., and Sanzhong, L.: Late Archean to Paleoproterozoic evolution of the North China Craton: key issues revisited, Precambrian Res., 136, 177–202, https://doi.org/10.1016/j.precamres.2004.10.002, 2005.

Zhao, L. and Zheng, T.: Using shear wave splitting measurements to investigate the upper mantle anisotropy beneath the North China

Craton: Distinct variation from east to west, Geophys. Res. Lett., 32, L10309, https://doi.org/10.1029/2005GL022585, 2005.

Zhu, R., Xu, Y., Zhu, G., Zhang, H., Xia, Q., and Zheng, T.: Destruction of the North China Craton, Sci. China Earth Sci., 55, 1565–1587, https://doi.org/10.1007/s11430-012-4516-y, 2012.

Ziegler, P. A. and Cloetingh, S.: Dynamic processes controlling evolution of rifted basins, Earth-Sci. Rev., 64, 1–50, https://doi.org/10.1016/S0012-8252(03)00041-2, 2004.

Zwaan, F. and Schreurs, G.: How oblique extension and structural inheritance influence rift segment interaction: Insights from 4D analog models, Interpretation, 5, SD119–SD138, https://doi.org/10.1190/INT-2016-0063.1, 2017.

Zwaan, F., Schreurs, G., Naliboff, J., and Buiter, S. J. H.: Insights into the effects of oblique extension on continental rift interaction from 3D analogue and numerical models, Tectonophysics, 693, 239–260, https://doi.org/10.1016/j.tecto.2016.02.036, 2016.

Zwaan, F., Chenin, P., Erratt, D., Manatschal, G., and Schreurs, G.: Competition between 3D structural inheritance and kinematics during rifting: Insights from analogue models, Basin Res., 34, 824–854, https://doi.org/10.1111/bre.12642, 2022.